DOI: 10.1002/((please add manuscript number))
Article type:Full Paper

Design and Response of High-Efficiency Planar Doped Luminescent Solar Concentrators using Organic-Inorganic Di-Ureasil Waveguides

*Adarsh Kaniyoor, Barry McKenna, Steve Comby and Rachel C. Evans**

Dr. Adarsh Kaniyoor, Barry McKenna, Dr. Steve Comby, Dr. Rachel C. Evans
School of Chemistry & CRANN, Trinity College Dublin, Dublin 2, Ireland
E-mail: raevans@tcd.ie

Keywords: luminescent solar concentrators, organic-inorganic hybrid materials, di-ureasils, Förster resonance energy transfer, optical efficiency

Luminescent solar concentrators (LSCs) offer significant potential for solar energy capture in the urban environment. Here, the first example of a planar, doped LSC using Lumogen Red (LR305) as the luminophore and a di-ureasil organic-inorganic hybrid as the waveguide is reported. The di-ureasil waveguide offers several advantages over organic polymer waveguides including facile solution-processing from benign solvents and extension of the absorption window through energy transfer. Spectral evaluation using absorption and photoluminescence spectroscopies is used to optimize the LSC composition, yielding optical efficiencies as high as 14.5% (300-800 nm). A power conversion efficiency (PCE) of 0.54% was obtained for the champion LSC coupled to a c-Si PV cell using the di-ureasil precursor as an optical glue to minimize interfacial losses. Finally, a simple figure of merit to evaluate the performance of LSC-solar cell composite systems is proposed that enables comparison of the actual improvement in the efficiency of solar cells due to the attachment of the LSC, irrespective of the LSC design, architecture or materials. A PCE of 17.4% for the solar cell in the emission region of the LSC is obtained, which is a remarkable improvement of ~40% over its AM 1.5G value.

1. Introduction

Widespread uptake of solar technologies as a renewable energy source requires innovative thinking about how it may be deployed most effectively in the broadest of settings. While traditional silicon-based photovoltaic (PV) panels are ideal for wide, open spaces in sunny climes, they translate less readily to the urban environment due to their structural inflexibility and reduced performance in diffuse light conditions. Luminescent solar concentrators (LSCs) are a promising complementary technology to conventional photovoltaics for use in the built environment.[1–4] In its most basic architecture, an LSC consists of a transparent waveguide plate embedded or coated with one or more luminescent species. These luminophores harvest solar radiation incident on the plate and re-emit it at longer wavelengths. Due to total internal reflection, a significant fraction of the emitted photons are trapped within the plate, and are waveguided to the edges, where small photovoltaic cells can be attached to convert these photons to electricity.[3,4] The spatial and spectral concentration achieved in LSCs can generate intense, narrow bandwidth light with wavelengths matching the bandgap of attached solar cells, thereby improving their performance.[5–7] More importantly, their colorful aesthetic appeal, lightweight structure and flexible form, and the ability to concentrate bright as well as diffuse daylight means that LSC panels could find applications in built-up locations that are unsuitable for the installation of conventional photovoltaic panels. As such, everyday fixtures such as office blocks, railway stations and shopping centers could be transformed into light-harvesting and electricity-generating machines through the application of an LSC coating.[3,8]

Originally proposed in the late 1970s,[9,10] LSCs have yet to come onto the market due to several intrinsic light-loss mechanisms that have thus far prevented practical devices from achieving their theoretical efficiencies.[3,4,11,12] For example, luminophores based on organic molecular dyes are susceptible to photodegradation, either through direct decomposition by

sunlight or subsequent attack by singlet oxygen or other residual active species in the waveguide matrix.[3,8] Moreover, organic luminophores often exhibit a small Stokes shift, which can lead to significant losses through self-absorption.[3] However, the materials revolution of the last two decades, particularly in the area of organic electronics, has led to the generation of a vast library of new luminophores (*e.g.* quantum dots,[7,13,14] dyes/conjugated polymers,[5,15–18] metal complexes[4,19,20]) to be explored for LSC devices for the first time. This has enabled many of the losses associated with the luminophore such as low emission quantum yields, self-absorption, and incomplete light-harvesting to largely be addressed.[13–20] In comparison, the choice of waveguide has received relatively little attention. The laws of reflection ensure a minimum loss of ~23-28 % by way of surface reflection and escape cone losses in planar waveguides.[10] These losses are primarily dependent on the refractive index (n_{wg}) of the host waveguide material and are minimum when n_{wg} is in the range of 1.5–2.5.[10] Although, this wide range of refractive indices allows the use of a variety of materials, the additional requirements of optical clarity and high transmittance have conventionally limited the waveguides used to ordinary glass (n_{wg} ~1.5) or plastics such as poly(methyl methacrylate) (PMMA, n_{wg} = 1.49) and polycarbonate (PC, n_{wg} = 1.59).[21,22] While use of frequency-selective filters,[23,24] stacked plates containing different luminophores,[25] and dye alignment[26] can mitigate these losses to some extent, there exists a huge potential to overcome waveguide losses through the implementation of unexplored materials whose optical and physicochemical properties are specifically tailored for LSC applications.

Several new materials and composites such as poly(lactic acid),[27] unsaturated polyester,[28] sol-gel glasses like silica-zirconia and silica-titania,[29] and organic-inorganic hybrids such as polysiloxanes,[30] silsesquioxanes,[31] and di-urethane-silica[32] have been proposed as potential alternatives to PMMA. Among these, the organic-inorganic hybrids are particularly attractive due to their ability to simultaneously exhibit properties of both components such as easy processability, tunability and mechanical stability.[33] They also have

excellent optical properties which have made them promising candidates for a number of optical applications such as phosphors, light emitting diodes, optical sensors etc.[34,35] Furthermore, they can be prepared in a variety of forms, from free-standing monoliths, to thin films and coatings, which ensure their compatibility with the most commonly adopted LSC architectures.

Recently, representatives from the ureasil family of class II organic-inorganic hybrids have been employed in LSC devices for the first time.[36,37] Ureasils are generally prepared from the reaction between a commercially-available polyetheramine (Jeffamine®) and a silica precursor (*e.g.* 3-(triethoxysilyl)propylisocyanate (ICPTES)), followed by hydrolysis and condensation of the silica network using sol-gel chemistry.[36,38] Through judicious selection of the organic polymer within the hybrid structure, ureasils have been tailored towards specific applications like solid-state electrolytes,[38] integrated optical substrates,[39] and electrochromic windows.[40] Tri-ureasils doped with β-diketonate-europium(III) complexes were demonstrated as effective light-harvesting coatings for LSCs in a thin film configuration, with theoretical calculations demonstrating that an optical conversion efficiency (η_{opt}) of ca. 9% could be achieved.[36] The related Eu(III)-doped di-ureasil hybrid was subsequently used as a coating for a PMMA-based optical fiber in a cylindrical LSC architecture.[37] An effective optical conversion efficiency of 20.7% in the absorbing spectral region (300-380 nm) of the active layer was reported.

Here, we report the first example of a planar, doped LSC architecture using the commercially-available perylene dye Lumogen Red (LR305) as the luminophore and a di-ureasil (d-U(600)) organic-inorganic hybrid as the waveguide. We demonstrate that the di-ureasil waveguide can undergo energy transfer to the luminophore, introducing the possibility of extending the light-harvesting window of the LSC and discuss how spectral estimation of loss modes in the LSC can provide a valuable tool to optimize the performance. Moreover, we reveal that the precursor material used to fabricate the di-ureasil waveguide can also be

applied as a two-part optical adhesive to couple silicon solar cells to the edges of the LSC. The LR305-d-U(600) doped LSC exhibits optical efficiencies that are competitive with champion LSCs based on LR305/PMMA, clearly demonstrating that organic-inorganic ureasil waveguides are viable alternatives to PMMA. Finally, we discuss the challenges associated with benchmarking the performance of different LSC constructs, particularly when comparing the enhancement in the power conversion efficiencies of coupled solar cells and propose a new approach to enable comparison of reported results, irrespective of LSC design, architecture or materials.

2. Results and Discussion

2.1. Fabrication of doped di-ureasil LSCs

Doped LSCs were fabricated through the incorporation of the perylene-based red-emitting organic luminophore Lumogen F Red 305 into the organic-inorganic hybrid di-ureasil waveguide, as illustrated in **Figure 1**. Although LR305, like other organic dyes, may never find application in viable LSCs due to its small Stokes shift, its high photoluminescence quantum yield (PLQY) of ~97%, solubility in common solvents and good photostability have made it a starting reference dye for lab-scale LSCs.[17,30,41] The di-ureasil hybrid is synthesized in a two-step process as reported previously.[39] In brief, the polyetheramine, Jeffamine® ED-600, is first reacted with ICPTES to obtain the organic-inorganic hybrid precursor, di-ureapropyltriethoxysilane (d-UPTES). Acid-catalyzed hydrolysis and condensation of the siliceous framework subsequently yields the di-ureasil (d-U(600)), see Figure S1. Introduction of the luminophore into the waveguide precursor is achieved by dissolving the dye in d-UPTES solution at different concentrations (0.001 to 0.05 wt.% with respect to weight of d-UPTES) prior to hydrolysis. The viscous LR305-d-UPTES solution is cast into a suitable mold, which upon gelation and aging, shrinks and results in the formation

of the free-standing doped LSC monolith. The thickness of the LSC can be controlled by the initial volume of d-UPTES and the dimensions of the mold.

2.2. Optical characteristics of the waveguide and luminophore

To be suitable as waveguides for LSCs, materials must exhibit high transmittance in the solar spectral region and an optimum refractive index of 1.5–2.5.[10] In **Figure 2a**, the measured transmittance in the UV/Vis/NIR spectral region of the undoped d-U(600) monolith (thickness ~3 mm) is presented and compared with those of ordinary glass and PMMA. The ASTM G173-03 reference solar spectrum for AM 1.5G conditions is also shown. d-U(600) exhibits an excellent transmittance of >80% in the visible/NIR region of the solar spectrum, which is comparable to PMMA and glass. Moreover, d-U(600) exhibits an extended spectral transmission window in the UV region up to 280 nm, in comparison to PMMA which absorbs all wavelengths below 360 nm. This introduces the possibility of harnessing a greater portion of the solar spectrum if d-U(600) is used in conjunction with a UV-absorbing luminophore. The corresponding absorption coefficients were determined using the transmission spectrum and the sample thickness and are shown in Figure S2. Between 300-400 nm, d-U(600) exhibits a comparable absorption coefficient to glass, decreasing from ~ 6 cm^{-1} to <1 cm^{-1} across this region. This is much lower than observed for PMMA (~24 cm^{-1}) in the near UV region. In the visible/NIR region, the absorption coefficients for d-U(600), PMMA and glass are similar at ~0.5 cm^{-1}.

The refractive index of the d-U(600) thin film is shown in **Figure 2b**. In the dye emission region of 600-650 nm, n_{wg} for d-U(600) is 1.49 which is comparable to that of most commonly used waveguide material, PMMA.[22] Doped LSCs are most commonly prepared by an injection-molding process, in which dye-incorporated PMMA pellets are melted and injected into a shaped mold to form the waveguide plate.[42] In comparison, d-U600 is prepared using mild, solution-based processing conditions, whilst simultaneously exhibiting

superior optical properties, making it and related organic-inorganic hybrid polymers attractive alternatives to PMMA as transparent waveguides for LSCs.

Interestingly, the di-ureasils are known to be moderately photoluminescent with photoluminescence quantum yields between 6-10%,[43] and display a characteristic blue emission under UV illumination. The photoluminescence edge emission spectrum of d-U(600) exhibits a broad emission band centered between 350-600 nm, which is characteristic of di-ureasils (**Figure 3a**). This emission has previously been assigned to radiative electron-hole recombination mediated by donor-acceptor pairs occurring at (i) localized oxygen defects in the siliceous nanodomains (purple-blue component centered at ~2.7-3.0 eV) and (ii) photo-induced proton transfer between NH_2^+ and N^- defects localized at the urea linkages (blue component centered at ~2.5-2.6 eV).[44,45] The emission maximum is strongly dependent on the excitation energy, red-shifting to longer wavelengths as λ_{ex} increases. A similar trend is observed in the corresponding excitation spectrum (see Figure S4 in SI). The undoped d-U(600) exhibits a moderate PLQY of 7(±1)%, which is in excellent agreement with the literature for di-ureasils prepared by hydrochloric acid catalysis.[43]

The significant spectral overlap between the emission spectrum of d-U(600) and the excitation spectrum of LR305 introduces the possibility of Förster resonance energy transfer (FRET) from the waveguide to the luminophore (Figure 3a). The Förster distance, R_0 (the donor-acceptor distance at which the FRET efficiency is 50%), was determined to be 2.7 nm from the experimental spectral overlap integral. Given the relatively high concentration and the intimate blending of the luminophore within the di-ureasil waveguide, it is highly probable that this proximity is achieved and thus, that FRET occurs between the di-ureasil and LR305. Moreover, confocal microscopy studies on di-ureasils doped with photoluminescent conjugated polyelectrolytes have previously shown that the luminophore forms isolated nanodomains that are homogeneously distributed throughout the hybrid.[46] Confirmation for the occurrence of FRET is obtained from the PL emission and excitation spectra of an LR305-

doped LSC (0.001 wt.%) recorded in the 90°/edge emission configuration (Figure 3b). Upon excitation at 340 nm, which is semi-selective for the di-ureasil, typical emission profiles of both the di-ureasil and luminophore are observed. The corresponding excitation spectrum selectively detected in the emission maximum of LR305 exhibits a small feature in the 320–380 nm region (inset of Figure 3b), which is characteristic of the di-ureasil absorption and is absent in the absorption/excitation spectrum of pure LR305 in dilute solution. This provides concrete evidence for the occurrence of FRET from the waveguide to the luminophore. Unlike PMMA, di-ureasils can absorb a portion of the solar spectrum at wavelengths below 350 nm, re-emitting it at wavelengths accessible to the luminophore absorption. It should be noted that since the luminophore has a high molar absorption coefficient (ε = 44,200 M^{-1} cm^{-1} at 567 nm for LR305 in THF, see Figure S5 in SI), it will be the primary absorber in regions of spectral overlap. Nonetheless, the occurrence of FRET between the waveguide and the luminophore introduces the possibility of extending the light-harvesting window of the LSC, which should deliver a significant improvement in the device performance.

2.3. Optical efficiencies of LR305-d-U(600) planar LSCs

The performance of a given LSC is generally quantified on the basis of the optical conversion efficiency, η_{opt}, which can be determined experimentally by measuring the optical power output at the edges of the LSC (OP_{out}) with respect to the total incident solar power (OP_{in}) according to the equation:[4]

$$\eta_{opt} = \frac{OP_{out}}{OP_{in}} \quad (1)$$

The experimental η_{opt} was determined for planar LR305-d-U(600) LSCs by illuminating the top surface with AM 1.5G simulated solar radiation and measuring the edge output using a spectroradiometer-integrating sphere system (see Experimental Section and Figure S6 in SI for further details). The average power spectra emitted by the 4 edges of each LSC under dark

background conditions are presented in **Figure 4** and the integrated power output values are tabulated in Table 1. The average OP_{out} (integrated area under the curve) increases with dye concentration and reaches a maximum in the 0.005-0.01 wt.% range. Above this concentration, the optical power decreases, probably due to concentration quenching and/or self-absorption. It was recently noted that although LR305 is resistant to aggregation-induced quenching in solid PMMA matrices,[47] it cannot be ruled out in siloxane materials due to the apolar nature of the alkyl shielded siloxane macromolecule.[30] The experimentally-obtained total optical efficiencies calculated from Equation 1 are shown in the inset of Figure 4.

The experimental η_{opt} can be further boosted by optimizing the measurement conditions. For example, the total integrated OP_{out} measured with an absorbing black background reaches a maximum of 64 mW at a dye concentration of 0.005 wt.%. This value can be increased dramatically to 101 mW by using a white scattering background which allows a portion of the transmitted light to be reflected back into the LSC (see Figure S9 in SI). This results in a concomitant increase in η_{opt} from 9.2% for the absorbing background to 14.5% for the white scattering background. Moreover, use of a scattering aluminum tape on three sides of the LSC can further increase the optical efficiency, with η_{opt} increasing significantly to 16.4% for the 0.005 wt.% sample under these conditions (see Table 1).

It must be noted here that the values of power output and efficiency quoted above represent the values in the input wavelength range of 300-800 nm. This range was chosen so that our values can be compared with literature values for LR305 in PMMA, since the C-H vibrations in PMMA can absorb wavelengths >750 nm.[24] The corresponding values for the power output and total optical efficiencies of LSCs under different experimental conditions measured in the 250–1050 nm (full AM 1.5G spectrum) spectral range are presented in Table S1 for comparison (see SI). As expected, η_{opt} values determined over the larger spectral range are somewhat lower (7.7%, 12.5% and 14.3% using an absorbing background, scattering

background or reflective tape, respectively for the 0.005 wt.% LSC). These observations raise two important considerations when aiming to design champion LSC devices. Firstly, the experimental η_{opt} is extremely dependent on the measurement conditions, which makes it challenging to benchmark performance against state-of-the-art LSCs. Secondly, while use of the full solar spectrum would clearly be most appropriate for evaluating η_{opt}, variations in the absorption profiles of different luminophores and waveguides make this practically unfeasible if one wishes to evaluate the performance of a specific LSC configuration against the rest of the field.

To benchmark the performance of the doped LR305-d-U(600) LSC under our experimental configuration, a reference thin film LSC was fabricated by spin coating a LR305-DPPA/MMA solution onto a PMMA waveguide (4 cm × 4 cm × 3 mm), followed by photopolymerisation. This is one of the most commonly encountered LSC configurations in the literature based on the LR305 dye.[48,49] The highest total η_{opt} that could be obtained for the thin film LSC in our experimental configuration using a scattering background was 11.4 %, which is significantly lower than the corresponding doped LSC (see Table 1). Since the refractive indices and transmittance of PMMA and d-U(600) are comparable, the higher optical efficiencies in d-U(600) could be due to either improved light transport and/or the enhanced contribution due to FRET. As can be inferred from Table 1, the undoped d-U(600) (0 wt.%) has a total edge output of 10 mW with a dark background, much higher than the 1.2 mW output from a blank PMMA slab of similar thickness. The corresponding full spectrum values for the blank PMMA and the reference LSC are presented in Figure S9 and Table S2 (see SI).

Comparison with the state-of-the art is challenging due to the lack of consistency in reporting performance parameters in the field. Experimental considerations often restrict researchers to a specific LSC architecture, excitation source and spectral range over which

η_{opt} may be calculated. Our optimized LR305-d-U(600) LSC (0.005 wt.%) has an η_{opt} of ~14.5% with a white scattering background, which is comparable to the η_{opt} (15%) for a champion LR305-mixed polyacrylate thin film on PMMA under similar measurement conditions and over a similar spectral range (350-750 nm).[48] The LR305-d-U(600) LSC also compares well to the few examples of ureasil-based LSC architectures in the literature. An impressive optical efficiency of 20.7% was recently reported for a Eu^{3+}-complex doped d-U(600) thin film coated on a cylindrical PMMA LSC in the absorbing spectral range of 300–380 nm.[37] However, this value reduces to 1.2% if the entire AM 1.5G spectrum is considered. A Eu^{3+}-doped bridged silsesquioxane-based thin film LSCs demonstrated an optical efficiency of 0.43% over the AM 1.5G spectral range. [31] In contrast, η_{opt} for our champion planar LR305-d-U(600) doped LSC is 7.7 % (black background) when determined across the AM 1.5G spectral range. This compares very favorably with the 7.1% efficiency reported for a single stack PMMA LSC (5 × 5 cm) incorporating a mixture of LR305 and Fluorescence Yellow CRS040 as the lumophores with back reflectors under AM 1.5G irradiation.[50] These trends allow us to make two key observations. Firstly, ureasil-type hybrids are remarkably versatile waveguide materials that can be applied to a variety of LSC architectures generating remarkable optical efficiencies. Secondly, consideration of the spectral range over which η_{opt} is calculated/reported is crucial.

2.4. Prominent loss modes in LR305-d-U(600) planar LSCs

The optical efficiency of LSCs is generally far below 100 %, due to the several loss modes that are present. These losses are well-modelled by the following expression: [3,4,51]

$$\eta_{opt}^{spectral} = (1-R)\cdot\eta_{LHE}\cdot\eta_{LQE}\cdot\eta_{Stokes}\cdot\eta_{trap}\cdot\eta_{SA}\cdot\eta_{tr} \quad (2)$$

Here the optical conversion efficiency is described in terms of the optical properties of the waveguide and the luminophore; we have designated this as spectral optical efficiency

($\eta_{opt}^{spectral}$) to distinguish it from the experimentally determined optical efficiency (η_{opt}). η_{LHE} is the light-harvesting efficiency of the luminophore, η_{LQE} is the photoluminescence quantum efficiency (cf. PLQY) of the luminophore in the waveguide and η_{Stokes} is the Stokes efficiency that is associated with the Stokes shift of the dye. The Fresnel's reflection coefficient R represents the reflection loss from the waveguide surface, the trapping efficiency, η_{trap}, is a measure of light trapped in the waveguide due to total internal reflection, and the transport efficiency of the waveguide, η_{tr} represents losses occurring during transport including losses due to scattering and other imperfections within the LSC plate excluding losses due to re-absorption occurring during propagation. Thus, the efficiency/performance of any waveguide should be looked at in terms of three factors R, η_{trap}, and η_{tr}. The term η_{SA} is the self-absorption efficiency that accounts for the re-absorption of emitted photons by neighboring dye molecules and therefore depends on both the luminophore and device architecture. Estimation of these losses is essential to understand the light transport in LSCs and to accordingly design better devices.

We first consider the waveguide contribution to the optical conversion efficiency, which is largely determined by the three terms, R, η_{trap} and η_{tr} as discussed earlier. The first two depend only on the refractive indices of the waveguide (n_{wg}) and the surrounding medium (n_{med}), as given by Equations 3 and 4, respectively:[4,11]

$$R = \left| \frac{n_{med} - n_{wg}}{n_{med} + n_{wg}} \right|^2 \tag{3}$$

$$\eta_{trap} = \sqrt{1 - \left(\frac{n_{med}}{n_{wg}} \right)^2} \tag{4}$$

With air as the surrounding medium (n_{med} = 1.00), it can be shown that d-U(600) (n_{wg} =1.49) loses ~3.9% of the incident radiation by surface reflection and traps η_{trap} ~74% of the light emitted as photoluminescence.

To investigate the contribution of transport losses due to the combined effect of light escaping from the waveguide and reabsorption in the di-ureasil waveguide, the optical power spectrum was collected at one of the edges (2.0 × 0.3 cm^2) of a longer slab (7.0 × 2.0 cm^2) following upon excitation with simulated solar radiation at an isolated spot (0.4 cm diameter) positioned at different distances from the sample edge. The optical power output is observed to decrease as the distance from the irradiation spot is increased, as shown in **Figure 5a** for the LR305-d-U(600)-0.005 wt.% doped LSC. A red-shift in the emission maximum from 632 to 654 nm is observed upon increasing the detection distance from 1 cm to 2 cm; at greater distances the emission maximum remains unchanged (Figure 5a, inset). This suggests that losses due to self-absorption are saturated for optical distances >2 cm and are discussed in further detail below. The optical losses as a function of distance were quantified in terms of the integrated power output (300-800 nm), as shown in **Figure 5b**. Both the doped and blank d-U(600) samples show almost identical optical power losses for optical distances >2 cm, clearly indicating that scattering and geometrical losses predominate at longer distances. We note that the absolute power loss values differ considerably due to absence of a luminophore in the latter sample. This trend suggests that in case of window-sized di-ureasil based LSCs, most of light incident at the center will not reach the edges, and hence are not practical use in the current format. A possible solution is the use of filters to reduce the intrinsic absorption of d-U(600) in the UV region; for example, the use of a 480 nm filter leads to a more gradual decrease in power, as shown in **Figure 5b**.

While the losses due to the waveguide have a considerable impact on the performance of an LSC, it is clear that the losses associated with the luminophore have a significantly higher effect. The primary loss modes associated with the luminophore are self-absorption, light-harvesting efficiency, Stokes shift and quantum yield, and of these, the first two have a significant impact on the output of LSCs. Self-absorption is defined as the re-absorption of emitted photons by neighboring luminophores due to the overlap of their absorption and

emission spectra.[3,24] It is experimentally identified by a decrease in emission intensity, a red-shift in the emission maximum and/or a change in the spectral shape. Elevated luminophore concentrations and long optical pathlengths within the waveguide can increase self-absorption significantly,[52] especially in doped LSC architectures such as the one described here.

The PL emission spectra of LR305-d-U(600) LSCs measured in the front-face configuration are shown in **Figure 6a**. Upon excitation at 440 nm, the doped LSCs exhibit the characteristic emission spectrum of LR305 in the red spectral region. For the lowest doping wt.%, a small red-shift (10 nm) in the emission maximum at 610 nm is observed compared to the solution phase spectrum. An additional red-shift of 10 nm is observed as the luminophore concentration increases from 0.001 to 0.05 wt.% in the LSC. In the front-face configuration, only photons which lie within the escape cone of the waveguide will be detected and as such re-absorption/re-emission processes are not expected to significantly affect this measurement. The minor red-shift with increasing concentration is thus attributed to an increase in weak molecular interactions (*e.g.* π-π stacking) and formation of *J*-aggregates, even though the possibility of minor self-absorption cannot be conclusively ruled out.[53]

In contrast, the corresponding edge emission spectrum, which captures the waveguided photoluminescence, clearly depicts the effects of self-absorption (Figure 6b). As the luminophore concentration increases from 0.001 to 0.05 wt.%, the emission spectrum undergoes a significant spectral distortion, which is accompanied by a loss of vibrational fine-structure and the emergence of a single broad band centered at 665 nm. Moreover, the maximum PL intensity clearly reaches a saturation point once a critical luminophore concentration is reached, indicating the onset of quenching effects (see insets of Figures 6a and 6b). This trend supports the observations above that self-absorption is the predominant loss mode at optical distances < 2 cm.

One of the methods used to estimate the self-absorption efficiency is to scale the observed edge emission spectrum to match the true emission spectrum of the luminophore in

dilute solution (A<0.1) at the long wavelength edge of the spectrum where no self-absorption occurs (see section S-IV(a) in SI for further details).[51,54] The ratio of the integrated scaled edge emission spectrum over the true emission spectrum gives the self-absorption efficiency (*i.e.* η_{SA} = 1 in the absence of self-absorption). As predicted by the Beer-Lambert law, η_{SA} decreases exponentially (*i.e.*, self-absorption increases) from 53% to 23% as the dye concentration and consequently absorbance (A) increases. This trend can be modelled by the fit $\eta_{SA} = 0.22 + 0.36\exp(-0.74A_{max})$ as shown in Figure 6c. Extrapolation to low absorbance values shows although self-absorption effects cannot be completely eliminated, they can be reduced to give a $\eta_{SA} = 0.58$. At elevated concentrations, self-absorption is inevitable for any luminophore whose absorption and emission spectra overlap, which leads to an intrinsic self-absorption efficiency of 22% for LR305 in d-U(600). Though this value is slightly lower than previously reported for LR305-PMMA based thin-film LSCs (intrinsic self-absorption efficiency = 34%), it must be noted that doped architectures inherently have higher self-absorption (lower efficiency) than the thin film configuration.[51]

The light-harvesting efficiency refers to the fraction of incident radiation that can be absorbed by the LSC and can be determined from comparing the absorption spectrum of the LSC and the solar spectrum.[51] The absorption spectra of LSCs and the calculation methodology are presented in Figures S12 and S13 (see SI). The blank d-U(600) waveguide does not significantly absorb wavelengths above 400 nm, whereas the absorption profiles of all doped LSCs exhibit features similar to that of LR305 dye solution, albeit red-shifted by 12 nm in the absorption maximum (λ_{abs}). The light-harvesting efficiency was determined for the solar simulator output (class ABB with an AM 1.5G filter) in two wavelength regions: 300–800 nm and 250–1050 nm (full solar spectrum). As shown in Figure 6c, the light harvesting efficiency of LSCs increases exponentially with the absorbance/dye concentration and can be modeled as $\eta_{LHE(300\text{-}800nm)} = 0.65 - 0.58\exp(-0.8A_{max})$ and $\eta_{LHE(200\text{-}1050nm)} = 0.5 - 0.45\exp(-$

0.8A_{max}). These values are in close agreement with values reported for LR305 in PMMA,[51] suggesting that the d-U(600) is equivalent to PMMA in its optical quality and that the absorption profile is unaffected by the device architecture, provided they contain comparable amounts of the luminophore.

The Stokes efficiency represents the net energy loss associated with photoluminescence due to competing non-radiative processes (e.g. vibrational relaxation). It is inherently linked to the self-absorption efficiency, η_{SA}, since a small Stokes shift will inevitably increase the probability of reabsorption. However, in flux (number of photons) based models, such as that considered here, the Stokes efficiency is an inconsequential loss mode: all emitted photons arriving at the slab edges should be converted to an equivalent number of electrons by attached PV cells, provided their energy exceeds the bandgap minimum. The luminescence quantum efficiency (η_{LQE}) (cf. PLQY) of the LSCs was determined following the standard procedure for solid samples[55] and corrected for reabsorption/remission processes as described by Ahn *et al* for optically-thick samples.[54] (Calculation details and values are provided in Section S-IV(c) in SI, Figure S13 and Table S3). The LSC with 0.005 wt.% dye has the highest PLQY of 88 (± 0.6)% which decreases moderately to ~77 % as the dye concentration increases to 0.05 wt.%.

This analysis reveals that the optical efficiency of planar LR305-d-U(600) LSCs is predominantly governed by the light-harvesting and self-absorption efficiencies, which depend mainly on the properties of the luminophore. From Figure 6c, it can be seen that at an absorbance in the region of ~0.9–1.4, the product of η_{LHE} and η_{SA} is maximum, and so will be η_{opt}. For large area LSCs, transport efficiency of the waveguide will also play an important role; although it must be noted that at low Stokes shift values, the isolation of self-absorption effects from the total transport efficiency is difficult and hence must be seen as one unit.[56]

2.5 Thermal and Photostability

The thermal and photostability of the waveguide and the lumophore-waveguide combination are important considerations for the lifetime of such devices. The thermograms for d-U(600) slab and the LR305-d-U(600)-0.005wt% LSC are in good agreement with each other (Figure S3) with the onset of sample decomposition observed at ~340℃. This thermal stability considerably surpasses the moderate operating temperatures (~65-140℃) present in organic electronic devices.[57] The photostability of the LR305-d-U(600)-0.005 wt% LSC and the d-U(600) waveguide was investigated by measuring their power output upon simulated solar illumination before and after the samples were exposed to UV irradiation (λ = 366 nm) for increasing periods of time (t = 0 to 24 hours). To ensure that any modulation of the power output can be associated with the UV-induced photodegradation of the sample, half of the slab was covered with a mask to avoid any exposure to UV light. As shown in **Figure 7**, the optical power of the LR305-d-U(600) slab decreases linearly with the irradiation time, while the optical power measured at the edge of the unexposed part of the sample remains constant throughout the entire experiment. After 15 h irradiation, the optical power decreases to 55% of the initial value, droping further still to down to 38% after 24 h. The same experiment performed on the d-U(600) did not result within experimental error in any decrease of the power output at increasing irradiation times. This behavior supports the hypothesis of degradation of the dye molecule in the doped LSC, in line with the mechanism previously reported by Griffini *et al*,[58] whilst simultaneously demonstrating the photostability of the d-U(600) waveguide. The LR305 photodegradation was further corroborated by measuring the absorption spectra of the exposed and unexposed part of the monolith. As already visible to the naked eye, a significant decrease in the absorption at 445 nm and in the 500-620 nm range is observed (Figure 7c). Concomitantly, the lower energy absorption band is blue-shifted by 8 nm from 580 nm before UV exposure to 572 nm after irradiation, which is in agreement with previous reports.[58] Even though the LR305-d-U(600) LSCs appear to undergo noticeable

photodegradation under the experimental conditions employed, it is important to emphasize here that the dose of UV irradiation that the LSCs have been exposed to is much higher than under normal sun conditions (24 h of UV irradiation at 366 nm is equivalent to > 10 days of continuous sunlight, see Experimental Section). For a country like Ireland, with relatively low sunshine hours, this would translate roughly to 2-3 months exposure in outside conditions.

2.5. LSC-Si photovoltaic cell (PV) composite system

To evaluate the practical application of LSCs, it is imperative to study the performance of LSC-PV cell composite system(s). The LSC-PV interface reflects an additional source of optical loss in these devices and excellent matching of the refractive index of the two components is key to minimizing this loss. Typically, optically clear adhesives, polymers, or silicone grease are used to attach the LSC to the PV cell,[4,51,59] but in many cases an air gap is used.[30,37] Even with good refractive index matching, the use of a general optical adhesive introduces two additional interfaces; use of an air gap avoids this but does not provide satisfactory optical coupling. The ideal solution would be to identify an optical glue that is chemically-identical to the waveguide material. Gratifyingly, we discovered that the d-UPTES precursor used to prepare the d-U(600) waveguide functions perfectly as a two-part optical adhesive (see experimental section). Since the refractive indices and chemical composition of the d-UPTES glue and the waveguide match, ideal optical coupling between the LSC and the solar cell can be expected, with no possibility of chemical abrasion of the waveguide.

A crystalline silicon PV cell (c-Si) was attached to the edge of the LR305-d-U(600) planar LSC (0.005 wt.% dye loading) exhibiting the highest optical efficiency using the above described di-ureasil glue, as shown in **Figure 8.** The c-Si PV cell, after providing wire contacts, has an average power conversion efficiency of ~12 %, under 1 Sun AM 1.5G

simulated solar radiation. The power conversion efficiency of the LSC-PV cell couple (η_{PCE}) is defined as:

$$\eta_{PCE} = \frac{I_{sc}.V_{oc}.FF}{Irr_{in}.A_{ill}} = \frac{EP_{out}}{OP_{in}} \quad (5)$$

where Irr_{in} refers to the total irradiation incident on the illuminated area (A_{ill}) of LSC; I_{sc}, V_{oc}, FF and EP_{out} are short-circuit current, open-circuit voltage, fill factor and output electrical power, respectively. The current-voltage characteristics of the device with absorbing and scattering backgrounds under AM 1.5G simulated illumination are presented in Figure 8 and data are tabulated in Table 2. The present LSC-Si device has a single edge electrical power output of 4.9 mW and therefore a PCE of 0.54 %, under scattering background conditions and over the entire AM 1.5G spectral range. While this value appears to be lower than the best LSC device using LR305 and Si cells (2.9 % for 2 c-Si solar cells attached to adjacent edges),[59] it must be noted that we do not utilize highly reflective bottom and side mirrors to make our measurements. Measurements performed under similar conditions to ours, have yielded comparable results. For example, an Eu^{3+}-doped d-U(600) based thin film cylindrical LSC attached to a Si photodiode has a PCE of 0.14%,[37] whereas LR305-doped polyxylylene (Parylene™) thin films on PMMA have efficiencies in the range 0.13–0.46%,[60] depending on the detector type (Si PV cell/photodiode). In these two examples, the photodiode/Si PV cell is coupled to the LSC either by an air gap or optical grease. The elevated performance of our LSC-Si device may thus be due in part to good optical coupling provided by the d-UPTES adhesive.

We propose that alternative approach to analyze and compare data between different LSC systems would be to assume identical solar cells attached to all the edges of the LSC and extrapolate the single edge PCE to a total power conversion efficiency ($\eta_{PCE}(total)$). This is line with the fact that optical efficiencies are always determined by considering the summed

contribution from all edges of the LSC. Thus, the total PCE for our best LSC would be 2.16% (see Table 2). In mathematical terms, this reduces to:

$$\eta_{PCE}(total) = \eta_{opt} \cdot \eta_{PV}(\lambda_{em}) \quad (6)$$

where $\eta_{PV}(\lambda_{em})$ is the efficiency of the attached solar cell in the emission spectral range of the LSC, distinct from its AM1.5 value $\eta_{PV}(AM1.5G)$. This equation is an obvious relation since the efficiency of a composite system can be expressed in terms of product of efficiencies of the components.

Using equation 6, $\eta_{PV}(\lambda_{em})$ can be determined since the other two terms are either measured or extrapolated from experimental data. It can then be related to the ratio:

$$E = \frac{\eta_{PV}(\lambda_{em})}{\eta_{PV}(AM1.5G)} \quad (7)$$

The factor E is useful figure of merit for evaluating the performance of an LSC, since it tells us about the actual improvement in the efficiency of solar cells due to the attachment of the LSC. This term is used in various forms across the LSC literature (see section S-V in SI for more information),[4,37,59,61] to compare results, irrespective of LSC design, architecture or materials. For example, E is related to the term η_{solar}/η_{pv} as $1/E$,[31,37] whereas the optical collection probability, P,[59] is given by $P = E\eta_{opt}$. Using this formalism, our LSC-Si system has $\eta_{PV}(\lambda_{em})$ = 17.3 % and E = 1.4, which is not only higher than many recent reports, but also comparable to best. For example, the recently developed Eu^{3+}-doped silsesquioxane and d-U(600)-based LSCs have E = 0.9[31] and 1.1[37], respectively, whereas, the best LR305-PMMA-Si LSCs have E = 1.2-2.4,[48,59] depending on the number of cells attached.

The effect of the parameter E on our LR305-d-U(600) planar LSC can also be equivalently discussed in terms of power output too. Under similar illumination conditions, a single edge of the 0.005 wt.% LSC produces 28.2 mW (scattering background, see Table S1)

of optical power, and a solar cell connected to this edge produces 4.9 mW of electrical power. This implies a power conversion efficiency of 17.4 % for the solar cell in the emission region of the LSC, which is a significant improvement of ~40 % over its A.M. 1.5 value of 12.2 %. Given the simple LSC configuration adopted here, these results suggest that significant improvements in the power conversion efficiency should be achievable if the device is further optimized (*e.g.* with filters and back-reflectors *etc.*).

3. Conclusions

With an optimum refractive index of 1.49 and transmittance of >80% in the visible region, we have shown that the d-U(600) di-ureasil organic-inorganic hybrid is a viable alternative to glass, polycarbonate or PMMA as a waveguide material for luminescent solar concentrators. Moreover, the simple, cheap and environmentally-friendly synthesis process used to prepare ureasil materials lends itself to the facile fabrication of LSCs in a variety of architectures (i.e. doped, thin film[36] and cylindrical[37]). In particular, the solution-based approach demonstrated here for the fabrication of doped LSCs offers a considerable advantage over the injection-moulding process currently used to fabricate PMMA-based doped LSCs. The moderate absorption of the di-ureasil in the UVA region (340-400 nm) of the solar spectrum can be effectively harnessed through energy transfer to the luminophore, thus reducing this loss mechanism in the waveguide compared to PMMA and effectively extending the light-harvesting window in the LSC. The d-U(600) waveguide exhibits a high thermal stability (>320 °C), which considerably exceeds both the typical operating temperatures reported for optoelectronic devices and realistic environmental exposure temperatures. It also exhibits a high photostability, showing no significant optical degradation under accelerated UV exposure (equivalent to 10 days continuous, direct sunlight exposure).

The highest experimental optical efficiency was obtained for a dopant concentration of 0.005 wt.% (η_{opt} =14.5%, spectral region 300-800 nm, scattering background). Notably, the d-

UPTES precursor can itself function as a two-part optical adhesive to adhere c-Si solar cells to the edges of the LSC. A power conversion efficiency of 0.54% was obtained for our champion LSC coupled to a c-Si PV cell along a single edge using the d-UPTES optical glue and in the absence of any additional reflective coatings. This PCE is as good as, or superior to values reported in the literature for the best comparable PMMA-based LSCs. Finally, we propose a simple figure of merit to evaluate the performance of LSC-solar cell composite systems that enables comparison of the actual improvement in the efficiency of solar cells due to the attachment of the LSC, irrespective of the LSC design, architecture or materials. This formalism indicates a power conversion efficiency of 17.4% for the solar cell in the emission region of the LR305-d-U(600)LSC, which is a significant improvement of ~40% over its AM 1.5G value of 12.2%. The results indicate that ureasil-based organic-inorganic hybrids are eminently suitable as waveguide materials for LSCs in diverse constructs. Moreover, a huge variety of Jeffamine™ precursors[62] are commercially-available, which also makes tuning of the mechanical properties of the waveguide possible (e.g. strength, flexibility, porosity). Advances in the design of optical materials will clearly play a significant role in bringing LSC technology to the commercial market.

4. Experimental Section

Materials: *O*, *O*'–bis(2-aminopropyl)polypropylene glycol–block– polyethylene glycol-block–polypropylene glycol (Jeffamine ED-600®), 3-(triethoxysilyl)propylisocyanate (ICPTES, purity 95%), methyl methacrylate (MMA, 99%), di-pentaerythriolpenta/hexa-acrylate (DPPA) and 1-hydroxycyclohexyl phenyl ketone (99 %) were purchased from Sigma Aldrich and used as received. All solvents were procured from Sigma Aldrich or Fischer Scientific and used without further purification. The luminophore Lumogen F Red 305 (LR305) was a generous gift from BASF, Germany. Monocrystalline silicon solar cells with active area of 4 cm × 0.3 cm and a 2 mm busbar were purchased from Solar Capture Technologies, U.K. Silver-loaded

epoxy conductive adhesive from Radionics Ltd. was used to put wire contacts on solar cells. PMMA plates (Marcryl) were purchased from 365 Plastics Ltd. and cut manually to 4 × 4 × 0.28 cm^3 pieces (refractive index = 1.491, density 1.19 g/cm^3). Glass slides were purchased from Erie Electroverre SA and comprised SiO_2 (72.2%), Na_2O (14.3%), CaO (6.4 %), MgO (4.3%) and trace amounts of other inorganic oxides (thickness = 10 mm, refractive index = 1.5171).

Fabrication of planar LR305-d-U(600)LSCs: The d-U(600) di-ureasil waveguides were prepared using a two-step process based on the method reported by Oliveira *et al*.[39] In the first step, a stock solution was prepared by mixing ICPTES (9.1 mL, 30.0 mmol) and Jeffamine ED-600 (10 mL, 17.5 mmol) in THF (50 mL) and refluxing at 70 °C for 12 h to obtain a stock solution of the hybrid precursor, di-ureapropyltriethoxysilane (d-UPTES). A volume equivalent to '10 batches' of d-UPTES was obtained by this process. The second step involves acid-catalyzed hydrolysis and condensation of the d-UPTES 'sol' to obtain the transparent di-ureasil, d-U(600). In a typical process (for 1 batch), ethanol (0.4 mL, 7 mmol) was added to d-UPTES (6.7 mL) solution under stirring. To this, aqueous HCl (0.04 mL, 0.5 M) was added, followed by the addition of de-ionised water (0.095 mL). The final molar ratio for the hydrolyzing solution of ethanol: HCl: water is 350:1:265.

To prepare undoped d-U(600) waveguides of 2.8 mm thickness, 4 batches of d-UPTES were required. The hydrolyzing mixture was added in appropriate quantity to initiate gelling. After stirring at room temperature for a few minutes, the gelling solution was poured into a polypropylene mould, which was then sealed with Parafilm® and left to dry. A slow aging/drying process involving room temperature drying and oven drying (40 °C) over a period of 1 week was used to obtain large monoliths (4.4 × 4.4 × 0.3 cm^3), which were then cut to the required size (4 × 4 × 0.3 cm^3). To fabricate luminophore-doped LSCs, the requisite volume of a stock solution of LR305 dye (5 mg/mL in THF) was added to the d-UPTES

solution prior to gelation to obtain dye-loadings of 0.001, 0.0025, 0.005, 0.01 and 0.05 wt.% (with respect to the mass of d-UPTES).

Fabrication of thin film LR-305-PMMA reference LSC: PMMA plates (4 × 4 cm^2) were cleaned by rinsing in soap water, followed by distilled water and ethanol. Acrylate resin (1000 µL), comprised of DPPA, MMA (5:1 weight ratio), LR305 dye (0.2 wt%) and 1-hydroxycyclohexyl phenyl ketone as a photoinitiator (0.3 wt.%), was heated to 65 °C and dropped onto a PMMA substrate (40 × 40 mm) and evenly spread across the surface before being spun at 1000 rpm for 30 s. The film was photopolymerized for 135s under UV-illumination from a 30 W UV grid lamp (254 nm) under N_2 flow. The film was then rinsed with ethanol to remove any unpolymerized excess. The film thickness determined using spectral reflectance measurements was found to be 21 µm.

c-Si PV cell attachment: Electrical contacts were given to the c-Si solar cell using silver loaded epoxy resin. The I-V characteristics of the solar cell were recorded after the addition of wire contacts, under AM 1.5G solar illumination. To couple the solar cell to the LSC, d-UPTES was used as a two-part adhesive. The precursor, d-UPTES (335 µL) in ethanol (20 µL, 0.34 mmol) formed the first component and the hydrolyzing solution of HCl (2 µL, 0.5 M) and water (4.7 µL, 0.26 mmol) formed the second. The two components are mixed maintaining the molar ratio of 340:1:260 ethanol: HCl: water, and left aside for a few minutes. When the mixture becomes sufficiently viscous, it is applied as a thin layer on the LSC edge and the solar cell is pressed against this edge. As the d-UPTES sol gels, it hardens and binds the solar cells. For complete curing, one day is required.

Characterization: UV/Vis absorption spectroscopy was carried out using both Perkin Elmer Lambda 35 UV/Vis and Lambda 1050 UV/Vis/NIR spectrophotometers at a scan speed of

240 nm/min and a slit width of 2 nm. For solutions, standard 10 mm quartz cuvettes were used, whereas the solid samples were directly inserted into the sample holder. For solid samples with very high absorbance, a Shimadzu UV2401 PC UV-Vis scanning spectrometer was used with similar measurement conditions.

Steady-state photoluminescence measurements were either performed on a Horiba Scientific Fluoromax–4 (solution-phase) or a Horiba Jobin Yvon Fluorolog-3 (solid-state) spectrophotometer. All emission and excitation spectra were corrected for the wavelength response of the system using correction factors supplied by the manufacturer. Solid-state emission spectra were recorded in both the front-face and edge emission configurations (detector at 15° and 90°, respectively). Typically emission and excitation slit widths were 1.5 and 0.5 nm, respectively. Solid-state PLQY measurements were performed using an integrating sphere and following the methodology of de Mello *et al*.[55] As the LR305-d-U(600) samples are optically thick, measured PLQY values were corrected for reabsorption/remission using the approach described by Ahn *et al*.[54] Full details can be found in the Supporting Information. The Förster radius, R_0, defined as the donor-acceptor distance at which FRET is 50% efficient was determined using the PhotochemCAD software.[63,64]

The refractive index of the d-U(600) di-ureasil was determined using a Filmetrics F20 thin film analyzer in the wavelength range 400 to 800 nm. A BK7 reflection standard was used to calibrate the instrument in the contact stage mode. The sample was prepared by spin coating d-U(600) on a glass substrate at 2000 rpm for 40s. The manufacturer-provided model was used to analyze the obtained results.

Thermogravimetric analysis (TGA) was performed using a Perkin Elmer Pyris 1 TGA thermogravimetric analyzer in the range 30-900 °C in an air atmosphere using *ca*. 2-5 mg sample, at a heating rate of 10 °C min^{-1} in a ceramic crucible. The instrument was calibrated against In and Ni standards in an air atmosphere.

Illumination of LSCs and solar cells was performed using a Class ABB solar simulator (Abet Technologies) equipped with an AM 1.5G filter. The illumination spot on the LSCs was defined by a black mask with a circular aperture of diameter 3.5 cm (area = 9.6 cm^2). The edge emission spectra of the LSCs were measured using an INS 125 integrating sphere coupled to an ILT 950 spectroradiometer. The linear attenuation length used to quantify the transport efficiency was measured using the experimental set-up shown in Figure S7. A black mask containing a circular irradiation aperture was used to isolate the irradiation spot (source is the solar simulator). The irradiation spot was moved at fixed distances across the sample surface to enable variation of the detection distance. The data were analyzed using Spectralight III software and the manufacturer provided calibration file ILT1007131U1INS125 for optical power measurements. Further details on the experimental set-up used to determine the optical power output of LSCs can be found in the Supporting Information. Current-voltage characterization of solar cells was performed using a Keithley 2401 source meter and the data acquisition was recorded using the Tracer 2 software. The output of the solar simulator was calibrated to 1 Sun (980 ± 40 Wm^{-2}) using a reference Si solar cell from ReRa Technologies and for confirmation, the output was also measured using the integrating sphere/spectroradiometer. The integrated power of the solar simulator over the exposed area of 9.6 cm^2 is 901 mW in the 250–1050 nm range and 699 mW in 300–800 nm range.

Accelerated photodegradation studies were carried out on both LR305-doped (0.005 wt%) and d-U(600) samples. The slabs were partially irradiated on one side at 366 nm using a UV lamp (Camag, Switzerland), while the other side was protected from any UV irradiation. The edge power output of both sides, irradiated or not, was measured at different irradiation times using the experimental setup described above. We note that only a single 0.4 cm diameter circle situated 2 cm away from the edge of the LSC was illuminated by the solar simulator to ensure that the light guided to the edge is coming exclusively from the photodamaged or

pristine area of the slab. The irradiation power of the UV source was quantified using a photodiode (Newport, 818-UV-L detector) coupled to a Keithley 2401 Sourcemeter in two probe mode with Tracer 2 software, yielding irradiance values of 7.72 Wm^{-2} at 366 nm. Knowing the actual solar power output (AM 1.5G) at 366 nm (0.735 W m^{-2}), an exposure time of 1 h with our UV source corresponds approximately to 10.5 h of solar irradiation.

Supporting Information
Supporting Information is available from the Wiley Online Library or from the author.

Acknowledgements

This work was supported by the Science Foundation Ireland under Grant No. 12/IP/1608.

Received: ((will be filled in by the editorial staff))
Revised: ((will be filled in by the editorial staff))
Published online: ((will be filled in by the editorial staff))

[1] W. G. J. H. M. van Sark, *Renew. Energy* **2013**, *49*, 207.

[2] D. Chemisana, *Renew. Sustain. Energy Rev.* **2011**, *15*, 603.

[3] M. G. Debije, P. P. C. Verbunt, *Adv. Energy Mater.* **2012**, *2*, 12.

[4] S. F. H. Correia, V. De Zea Bermudez, S. J. L. Ribeiro, P. S. André, R. A. S. Ferreira, L. D. Carlos, *J. Mater. Chem. A* **2014**, *2*, 5580.

[5] V. Sholin, J. D. Olson, S. A. Carter, *J. Appl. Phys.* **2007**, *101*, 123114.

[6] X. Huang, S. Han, W. Huang, X. Liu, *Chem. Soc. Rev.* **2013**, *42*, 173.

[7] C. S. Erickson, L. R. Bradshaw, S. McDowall, J. D. Gilbertson, D. R. Gamelin, D. L. Patrick, *ACS Nano* **2014**, *8*, 3461.

[8] V. Wittwer, W. Stahl, A. Goetzberger, *Sol. Energy Mater.* **1984**, *11*, 187.

[9] W. H. Weber, J. Lambe, *Appl. Opt.* **1976**, *15*, 2299.

[10] A. Goetzberger, W. Greubel, *Appl. Phys.* **1977**, *14*, 123.

[11] J. S. Batchelder, A. H. Zewail, T. Cole, *Appl. Opt.* **1979**, *18*, 3090.

[12] G. Smestad, H. Ries, R. Winston, E. Yablonovitch, *Sol. Energy Mater.* **1990**, *21*, 99.

[13] I. Coropceanu, M. G. Bawendi, *Nano Lett.* **2014**, *14*, 4097.

[14] F. Meinardi, A. Colombo, K. A. Velizhanin, R. Simonutti, M. Lorenzon, L. Beverina, R. Viswanatha, V. I. Klimov, S. Brovelli, *Nat. Photonics* **2014**, *8*, 392.

[15] B. J. Bruijnaers, A. P. H. J. Schenning, M. G. Debije, *Adv. Opt. Mater.* **2015**, *3*, 257.

[16] Y. Zhao, G. A. Meek, B. G. Levine, R. R. Lunt, *Adv. Opt. Mater.* **2014**, *2*, 606.

[17] M. G. Debije, P. P. C. Verbunt, P. J. Nadkarni, S. Velate, K. Bhaumik, S. Nedumbamana, B. C. Rowan, B. S. Richards, T. L. Hoeks, *Appl. Opt.* **2011**, *50*, 163.

[18] J. ter Schiphorst, A. M. Kendhale, M. G. Debije, C. Menelaou, L. M. Herz, A. P. H. J. Schenning, M. Laura, A. P. H. J. Schenning, *Chem. Mater.* **2014**, *26*, 3876.

[19] K. Binnemans, *Chem. Rev.* **2009**, *109*, 4283.

[20] X. Wang, T. Wang, X. Tian, L. Wang, W. Wu, Y. Luo, Q. Zhang, *Sol. Energy* **2011**, *85*, 2179.

[21] P. S. Friedman, *Opt. Eng.* **1981**, *20*, 887.

[22] M. J. Kastelijn, C. W. M. Bastiaansen, M. G. Debije, *Opt. Mater. (Amst).* **2009**, *31*, 1720.

[23] D. K. G. De Boer, L. Chi-Wen, M. P. Giesbers, H. J. Cornelissen, M. G. Debije, P. P. C. Verbunt, D. J. Broer, *Appl. Phys. Lett.* **2011**, *98*.

[24] B. C. Rowan, L. R. Wilson, B. S. Richards, *IEEE J. Sel. Top. Quantum Electron.* **2008**, *14*, 1312.

[25] A. A. Earp, G. B. Smith, J. Franklin, P. Swift, *Sol. Energy Mater. Sol. Cells* **2004**, *84*, 411.

[26] P. P. C. Verbunt, A. Kaiser, K. Hermans, C. W. M. Bastiaansen, D. J. Broer, M. G. Debije, *Adv. Funct. Mater.* **2009**, *19*, 2714.

[27] V. Fattori, M. Melucci, L. Ferrante, M. Zambianchi, I. Manet, W. Oberhauser, G. Giambastiani, M. Frediani, G. Giachi, N. Camaioni, *Energy Environ. Sci.* **2011**, *4*, 2849.

[28] Y. S. Lim, C. K. Lo, G. B. Teh, *Renew. Energy* **2012**, *45*, 156.

[29] F. Rey-García, C. Gómez-Reino, M. T. Flores-Arias, G. F. De La Fuente, A. Durán, Y. Castro, *Thin Solid Films* **2011**, *519*, 7982.

[30] M. Buffa, S. Carturan, M. G. Debije, A. Quaranta, G. Maggioni, *Sol. Energy Mater. Sol. Cells* **2012**, *103*, 114.

[31] V. T. Freitas, L. Fu, A. M. Cojocariu, X. Cattoën, J. R. Bartlett, R. Le Parc, J.-L. Bantignies, M. Wong Chi Man, P. S. André, R. A. S. Ferreira, L. D. Carlos, *ACS Appl. Mater. Interfaces* **2015**, *7*, 8770.

[32] R. Reisfeld, V. Levchenko, T. Saraidarov, *Polym. Adv. Technol.* **2011**, *22*, 60.

[33] P. Gomez-Romero, *Adv. Mater.* **2001**, *13*, 163.

[34] L. D. Carlos, R. A. S. Ferreira, V. de Zea Bermudez, B. Julián-López, P. Escribano, *Chem. Soc. Rev.* **2011**, *40*, 536.

[35] L. D. Carlos, R. A. S. Ferreira, V. de Zea Bermudez, S. J. L. Ribeiro, *Adv. Mater.* **2009**, *21*, 509.

[36] M. M. Nolasco, P. D. M. Vaz, V. T. Freitas, P. P. Lima, P. S. André, R. A. S. Ferreira, P. D. M. Vaz, P. Ribeiro-Claro, L. D. Carlos, *J. Mater. Chem. A* **2013**, *1*, 7339.

[37] S. F. H. Correia, P. P. Lima, P. S. André, M. R. S. Ferreira, L. A. D. Carlos, *Sol. Energy Mater. Sol. Cells* **2015**, *138*, 51.

[38] M. M. Silva, S. C. Nunes, P. C. Barbosa, A. Evans, V. de Zea Bermudez, M. J. Smith, D. Ostrovskii, *Electrochim. Acta* **2006**, *52*, 1542.

[39] D. C. Oliveira, A. G. Macedo, N. J. O. Silva, C. Molina, R. A. S. Ferreira, P. S. Andre, K. Dahmouche, V. de Zea Bermudez, Y. Messaddeq, S. J. L. Ribeiro, L. D. Carlos, *Chem. Mater.* **2008**, *20*, 3696.

[40] S. C. Nunes, V. de Zea Bermudez, M. M. Silva, M. J. Smith, D. Ostrovskii, R. A. S. Ferreira, L. D. Carlos, J. Rocha, A. Gonçalves, E. Fortunato, *J. Mater. Chem.* **2007**, *17*, 4239.

[41] R. Kinderman, L. H. Slooff, A. R. Burgers, N. J. Bakker, A. Büchtemann, R. Danz, J. A. M. van Roosmalen, *J. Sol. Energy Eng.* **2007**, *129*, 277.

[42] K. Bhaumik, J. D. Hurst, P. J. Nadkarni, N. Sankaran, S. Velate, (SABIC Innovative Plastics IP B.V.), Luminescent solar collector. *US 8304647 B2* **2012**.

[43] L. Fu, R. A. Sá Ferreira, N. J. O. Silva, L. D. Carlos, V. de Zea Bermudez, J. Rocha, *Chem. Mater.* **2004**, *16*, 1507.

[44] L. D. Carlos, R. A. Sá Ferreira, R. N. Pereira, M. Assunção, V. de Zea Bermudez, *J. Phys. Chem. B* **2004**, *108*, 14924.

[45] S. S. Nobre, P. P. Lima, L. Mafra, R. A. Sá Ferreira, R. O. Freire, L. Fu, U. Pischel, V. de Zea Bermudez, O. L. Malta, L. D. Carlos, *J. Phys. Chem. C* **2007**, *111*, 3275.

[46] N. Willis-Fox, A. T. Marques, J. Arlt, U. Scherf, L. A. D. Carlos, H. D. Burrows, R. Evans, *Chem. Sci.* **2015**, *x*, x.

[47] R. O. Al-Kaysi, T. Sang Ahn, A. M. Müller, C. J. Bardeen, *Phys. Chem. Chem. Phys.* **2006**, *8*, 3453.

[48] P. T. M. Albers, C. W. M. Bastiaansen, M. G. Debije, *Sol. Energy* **2013**, *95*, 216.

[49] W. G. J. H. M. van Sark, K. W. J. Barnham, L. H. Slooff, A. J. Chatten, A. Büchtemann, A. Meyer, S. J. McCormack, R. Koole, D. J. Farrell, R. Bose, E. E. Bende, A. R. Burgers, T. Budel, J. Quilitz, M. Kennedy, T. Meyer, C. D. M. Donegá, A. Meijerink, D. Vanmaekelbergh, *Opt. Express* **2008**, *16*, 21773.

[50] L. H. Slooff, E. E. Bende, A. R. Burgers, T. Budel, M. Pravettoni, R. P. Kenny, E. D. Dunlop, A. Büchtemann, *Phys. Stat. Sol. (RRL)* **2008**, *2* , 257–259.

[51] T. Dienel, C. Bauer, I. Dolamic, D. Brühwiler, *Sol. Energy* **2010**, *84*, 1366.

[52] R. W. Olson, R. F. Loring, M. D. Fayer, *Appl. Opt.* **1981**, *20*, 2934.

[53] L. R. Wilson, B. C. Rowan, N. Robertson, O. Moudam, A. C. Jones, B. S. Richards, *Appl. Opt.* **2010**, *49*, 1651.

[54] T. S. Ahn, R. O. Al-Kaysi, A. M. Müller, K. M. Wentz, C. J. Bardeen, *Rev. Sci. Instrum.* **2007**, *78*, 086105.

[565] J. C. de Mello, H. F. Wittmann, R. H. Friend, *Adv. Mater.* **1997**, *9*, 230.

[56] J. W. E. Wiegman, E. Van Der Kolk, *Sol. Energy Mater. Sol. Cells* **2012**, *103*, 41.

[57] I. T. Sachs-Quintana, T. Heumüller, W. R. Mateker, D. E. Orozco, R. Cheacharoen, S. Sweetnam, C. J. Brabec, M. D. McGehee, *Adv. Funct. Mater.* **2014**, *24*, 3978.

[58] G. Griffini, L. Brambilla, M. Levi, M. Del Zoppo, S. Turri, *Sol. Energy Mater. Sol. Cells* **2013**, *111*, 41.

[59] L. Desmet, A. J. M. Ras, D. K. G. de Boer, M. G. Debije, *Opt. Lett.* **2012**, *37*, 3087.

[60] G. Maggioni, A. Campagnaro, S. Carturan, A. Quaranta, *Sol. Energy Mater. Sol. Cells* **2013**, *108*, 27.

[61] C.-H. Chou, J.-K. Chuang, F.-C. Chen, *Sci. Rep.* **2013**, *3*, 2244.

[62] Huntsman International LLC, Products, http://www.huntsman.com/performance_products/a/Products.

[63] H. Du, R.-C. A. Fuh, J. Li, L. A. Corkan, J. S. Lindsey, *Photochem. Photobiol.* **1998**, *68*, 141.

[64] J. M. Dixon, M. Taniguchi, J. S. Lindsey, *Photochem. Photobiol.* **2005**, *81*, 212.

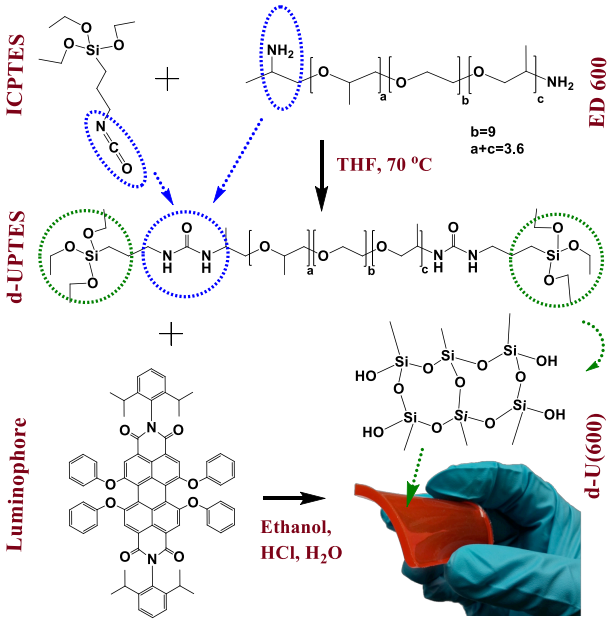

Figure 1. Schematic representation of the fabrication of LSC. In the first step, the precursors Jeffamine ED-600 and ICPTES are reacted to obtain di-ureapropyltriethoxysilane (d-UPTES). Following the dissolution of the luminophore, LR305 in d-UPTES, acid-catalyzed hydrolysis and condensation of the siliceous network is initiated to obtain the LR305-d-U(600) LSC. A picture of fabricated LSC is shown in the right corner.

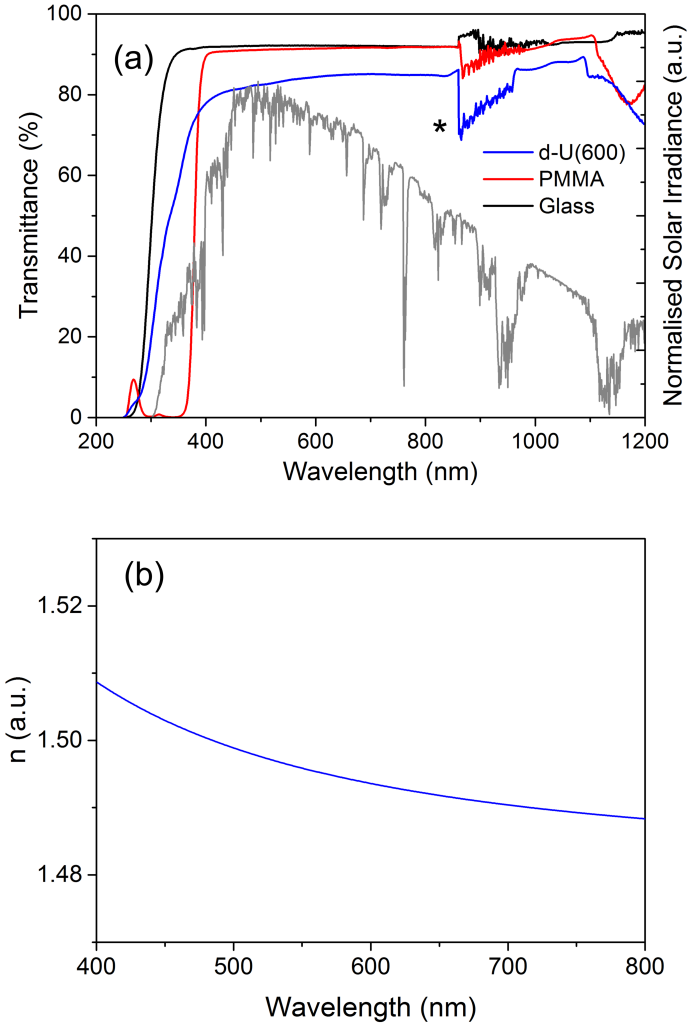

Figure 2. (a) Optical transmittance in the UV/VIS/NIR region of waveguide slabs made of d-U(600) (blue), PMMA (red) and glass (black). The AM 1.5G solar irradiance is shown in the background (grey). * Change of lamp. (b) Refractive index of d-U(600) across the visible region (400-800 nm).

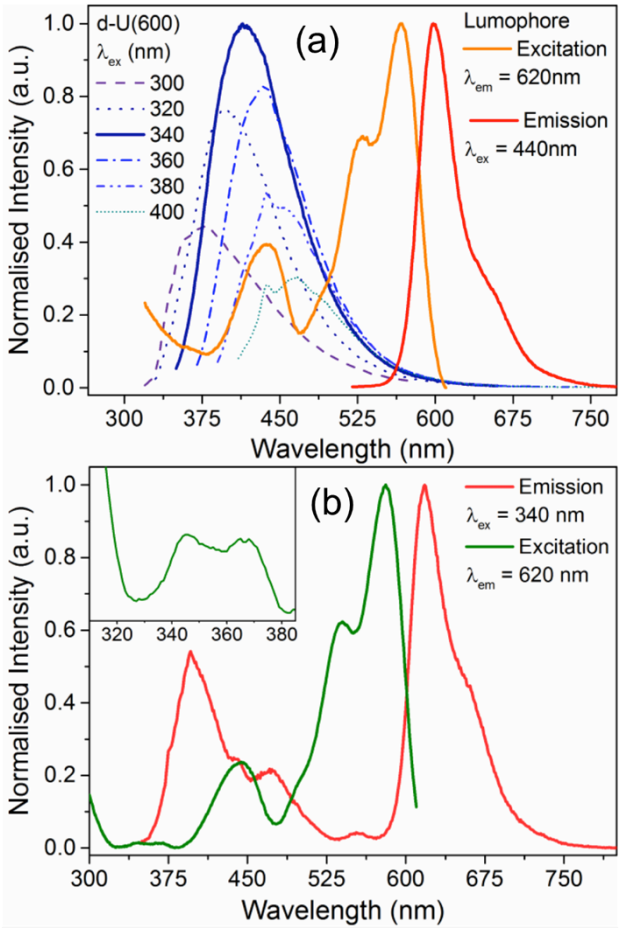

Figure 3. (a) Photoluminescence (PL) emission spectra of d-U(600) at different excitation wavelengths (blue) and PL excitation (orange) and emission (red) spectra of LR305 solution in THF (2 μM). (b) PL emission and excitation spectra of LR305-d-U(600) LSC (0.005 wt%). The sample was excited at 340 nm, the emission maximum of the di-ureasil, resulting in emission from both the di-ureasil and lumogen dye.

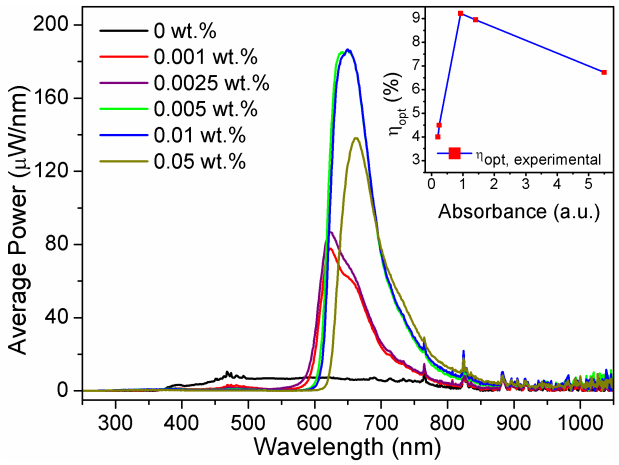

Figure 4. Optical power spectra of doped LR305-d-U(600) LSCs with a dark absorbing background, averaged over all four edges. (Inset) Variation of the experimental optical (red squares) efficiencies of the LSCs with a dark background, determined over the 300–800 nm spectral range, with respect to the LSC absorbance.

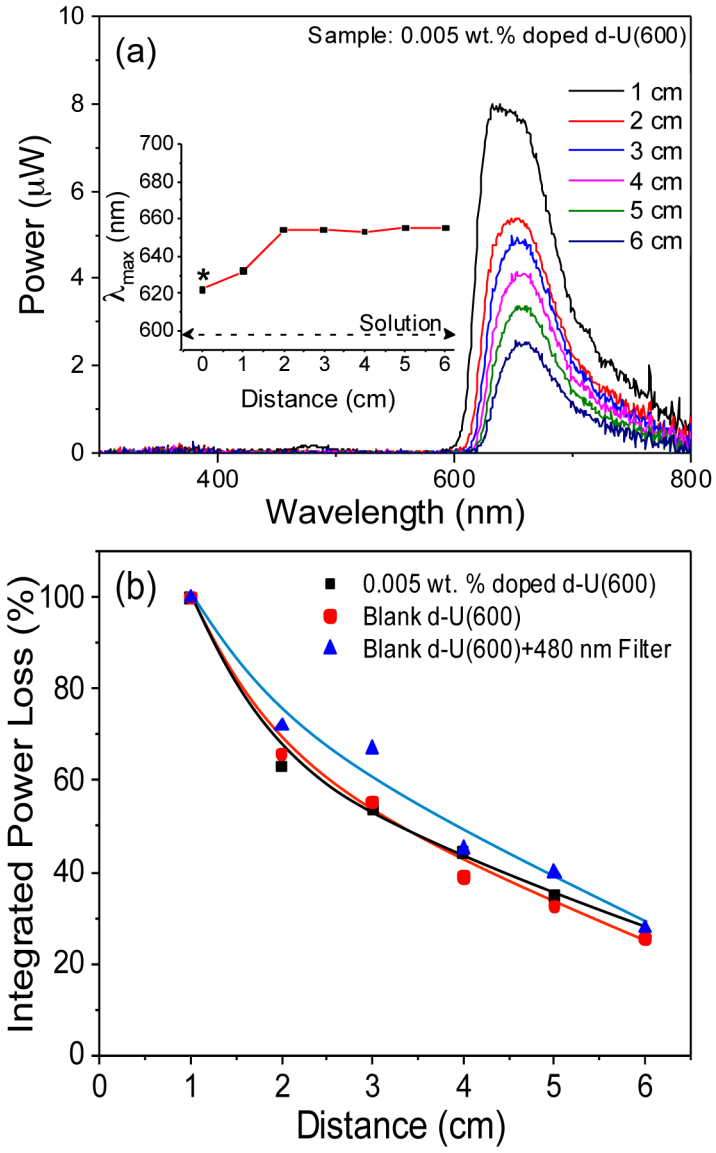

Figure 5. (a) Edge output spectrum of a LR305-d-U(600)-0.005 wt% slab with white scattering background collected at the edge of the LSC when the excitation spot is located at an increasing distance from the edge. Inset: Variation of emission maximum, λ_{max}, with distance from LSC edge, * denotes the λ_{max} for the lowest concentration LSC (0.001 wt%) which is used to approximate the zero distance value. The λ_{max} of a dilute solution of the luminophore where self-absorption should not contribute is represented by the dashed line.(b) Integrated power loss for the LR305-d-U(600)-0.005 wt% LSC and undoped d-U(600) slab as a function of distance. The corresponding power loss for the undoped d-U(600) slab obtained under the same conditions but using a 480 nm cut-off filter to attenuate UV/blue wavelengths is also shown. The solid lines serve only to guide the eye.

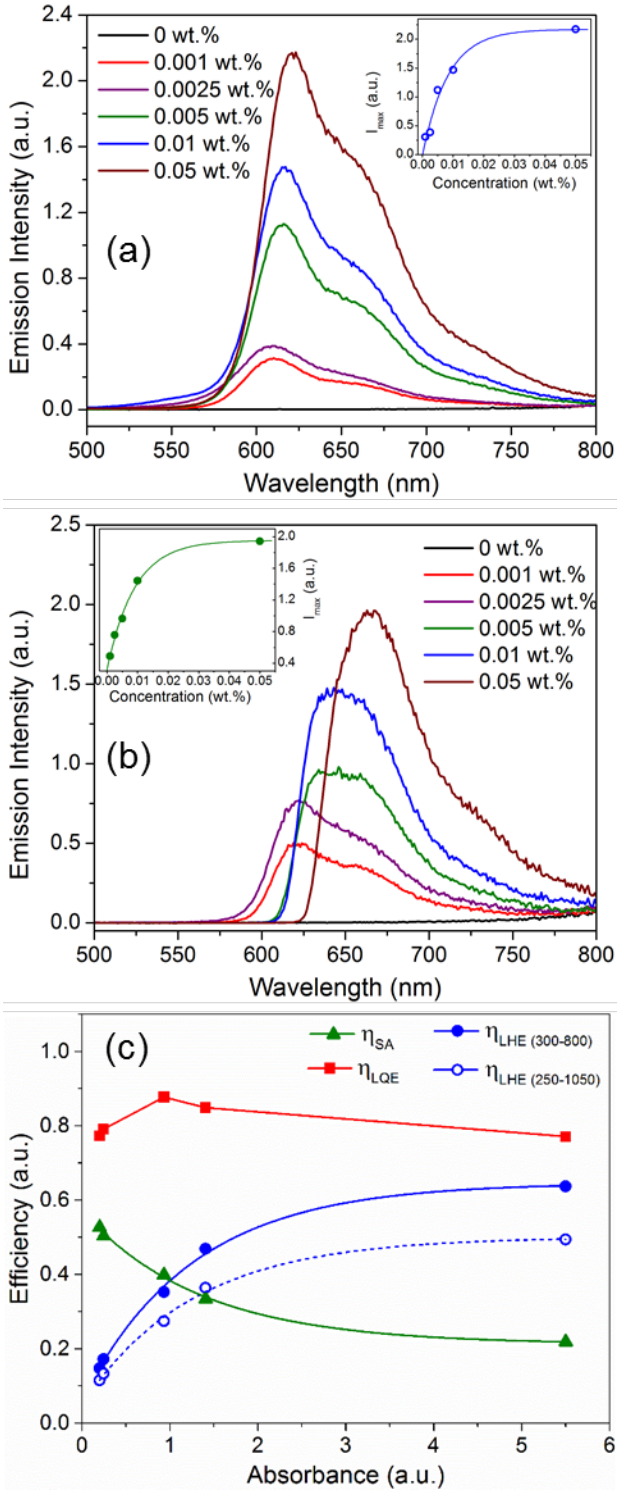

Figure 6. Photoluminescence emission spectra of LR305-d-U(600) LSCs in (a) front face configuration and (b) edge emission configuration. Insets: The respective insets show the variation of maximum PL intensity (I_{max}) with dye concentration. The solid line serves only to guide the eye. (c) Spectrally-determined efficiencies of LSCs, namely, light-harvesting (LHE, blue circles), self-absorption efficiencies (SA, green triangles), and luminescence quantum efficiencies (LQE, red squares) plotted against their absorbance values. The lines passing the points (LHE and SA) represent exponential fits as described in the text.

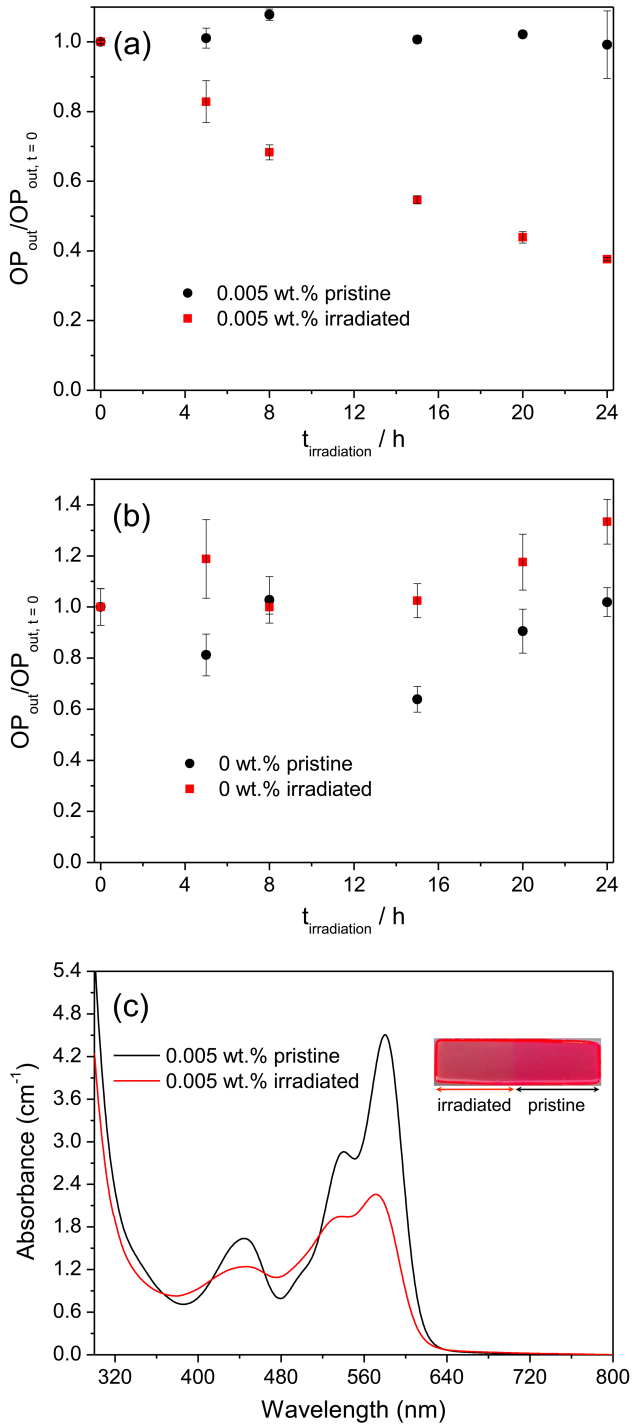

Figure 7. Optical power output measured at the edge of (a) the LR305-d-U(600)-0.005 wt.% LSC and (b) the d-U(600) waveguide for pristine and exposed side of the slabs at increasing irradiation times using UV light (366 nm). (c) UV/Vis absorption spectra of the LR305-d-U(600)-0.005 wt.% measured on the pristine and exposed ($t_{irradiation}$ = 24 h) side of the slab. The inset shows a picture of the slab and the clear difference in color of the irradiated and non-irradiated sides.

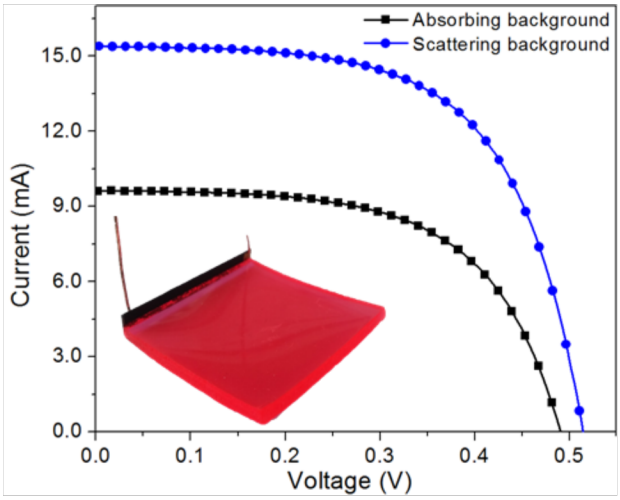

Figure 8. Current-voltage characteristics of c-Si solar cell coupled to 0.005 wt.% LR305-d-U(600) LSC under absorbing and scattering background conditions. A photograph of this sample is shown in the inset.

Table 1. Average power output from the edges of doped LR305-d-U(600) LSCs with different backgrounds and the corresponding total optical efficiencies determined in wavelength range 300–800 nm.

	Absorbing Background		Scattering Background		Scattering Back + Al tape	
Sample Code	Avg. Single Edge Output [mW]	Total Optical Efficiency [%]	Avg. Single Edge Output [mW]	Total Optical Efficiency [%]	Avg. Single Edge Output [mW]	Total Optical Efficiency [%]
0 wt.%	2.5	1.4	8.9	5.1	-	-
0.001 wt.%	7.0	4.0	14.8	8.5	20.6	11.8
0.0025 wt.%	7.9	4.5	15.3	8.7	-	-
0.005 wt.%	16.1	9.2	25.3	14.5	28.6	16.4
0.01 wt.%	15.6	8.9	22.4	12.8	22.9	13.1
0.05 wt.%	11.8	6.7	16.3	9.3	16.3	9.3
PMMA [a)]	0.3	0.2	1.7	1.0	-	-
Ref. LSC[b)]	11.4	6.5	19.9	11.4	20.8	11.9

a) Blank PMMA waveguide, b) Reference LSC: LR305 doped PMMA film on PMMA

Table 2. Current-voltage characteristics of LR305-d-U(600)-solar cell system (0.05 wt%).

Sample	I_{sc} [mA][a)]	V_{oc} [V][a)]	FF [a.u.][a)]	Electrical P_{out} [mW]	η_{PCE} [%]	η_{PCE}(total) [%]	$\eta_{PV}(\lambda_{em})$ [%]	$E = \eta_{PV}(\lambda_{em})/\eta_{PV}$(AM1.5G)
LSC-Si[b)]	15.4	0.514	0.618	4.89	0.54	2.16	17.3	1.42
LSC-Si [c)]	9.63	0.491	0.598	2.83	0.31	1.24	16.1	1.28
Si	42.1	0.534	0.649	14.59	12.16	-	-	-

[a)] I_{sc}, V_{oc} and FF are the short circuit current, open circuit voltage and fill factor, respectively;
[b)]scattering background; [c)]absorbing background

Design and Response of High-Efficiency Planar Doped Luminescent Solar Concentrators using Organic-Inorganic Di-Ureasil Waveguides

Adarsh Kaniyoor, Barry McKenna, Steve Comby and Rachel C. Evans*

ToC figure

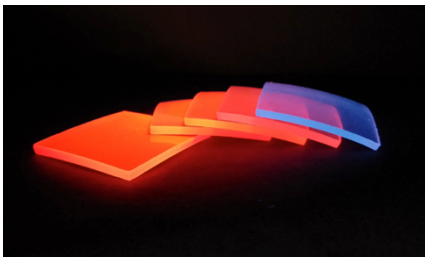

Planar doped luminescent solar concentrators exhibiting high optical concentration efficiencies are created using an organic-inorganic hybrid waveguide. The di-ureasil waveguide extends the spectral absorption window through energy transfer and functions as an optical adhesive to minimize interface losses. Selective engineering of the LSC composition through spectral evaluation yields a high optical efficiency of 14.5% (300-800 nm) and a power conversion efficiency of 0.54% upon coupling to a c-Si PV cell.

Supporting Information

Design and Response of High-Efficiency Planar Doped Luminescent Solar Concentrators using Organic-Inorganic Di-Ureasil Waveguides

Adarsh Kaniyoor, Barry McKenna, Steve Comby and Rachel C. Evans *

Table of Contents

S-I. Structure and optical properties of the di-ureasil hybrid waveguide

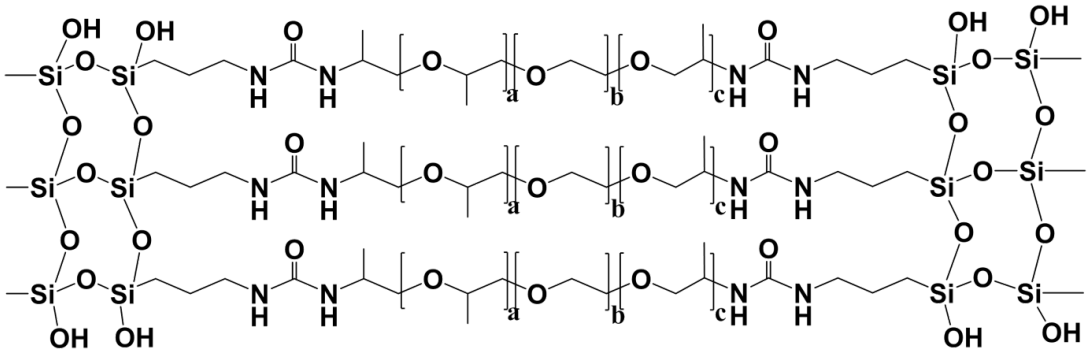

Figure S1. A partial representation of the d-U(600) structure indicating the organic component trapped between the inorganic siliceous backbone.

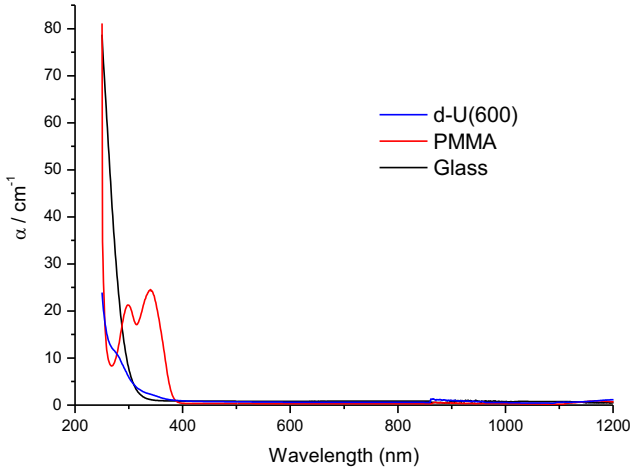

Figure S2. Absorption coefficient (α) for waveguide slabs determined from the transmission spectrum and the sample thickness.

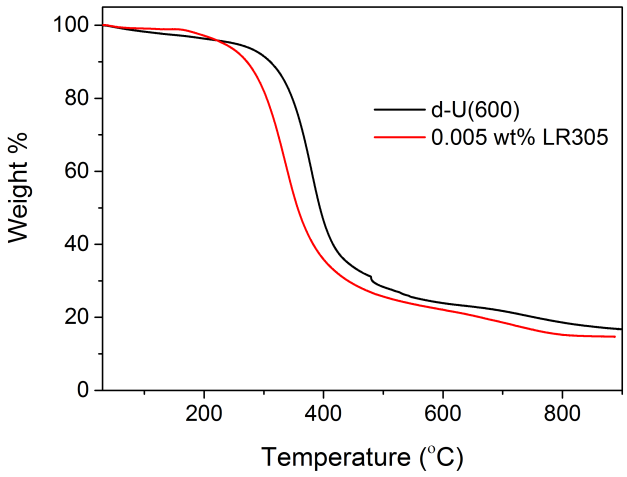

Figure S3. TGA thermograms of d-U(600) (black line) and LR305-d-U(600)-0.005wt% (red line). TGA measurements were performed in air at a heating rate of 10 °C min^{-1}.

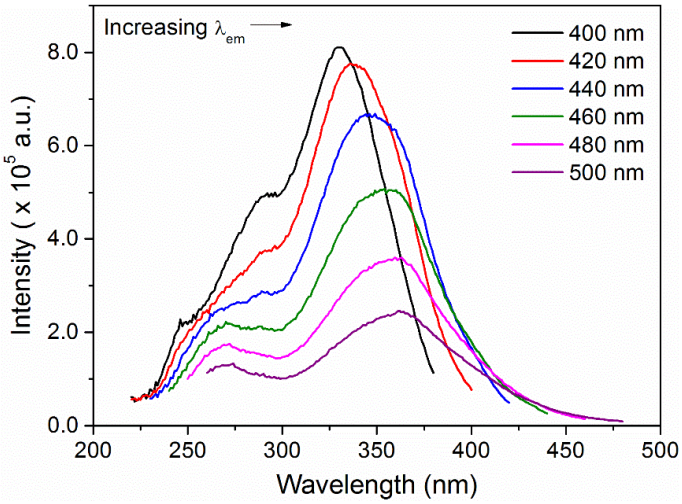

Figure S4. Photoluminescence excitation spectra of the d-U(600) monolith at different excitation wavelengths. The data were recorded in a 90°/edge emission configuration in the spectrophotometer.

S-II. Optical properties of Lumogen F Red 305 (LR305)

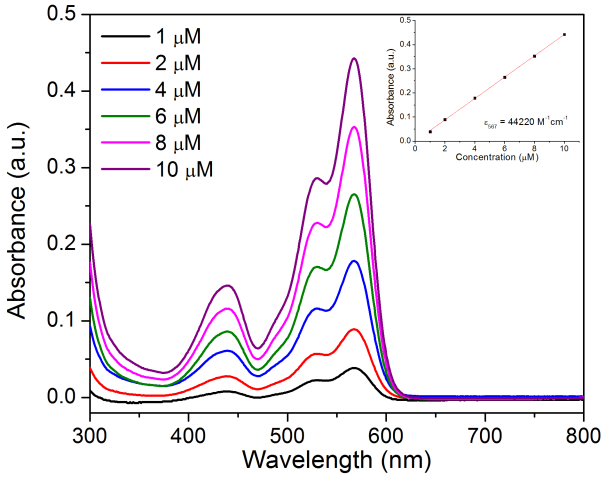

Figure S5. UV/Vis absorption spectra of LR305 at different molar concentrations in THF. (Inset) Beer-Lambert plot for LR305.

The experimentally determined molar extinction coefficients for LR305 dye are: 44220 $M^{-1}cm^{-1}$at 567 nm and 14450 $M^{-1}cm^{-1}$ at 440 nm.

S-III. Experimental characterization of the optical efficiency of LSCs

(a) Experimental Setup

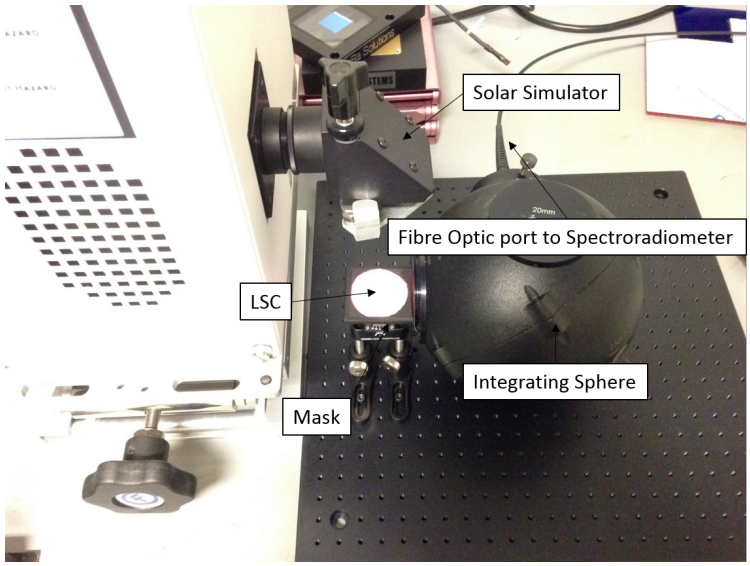

Figure S6. Experimental set-up for for the determination of the optical power output of LSCs.

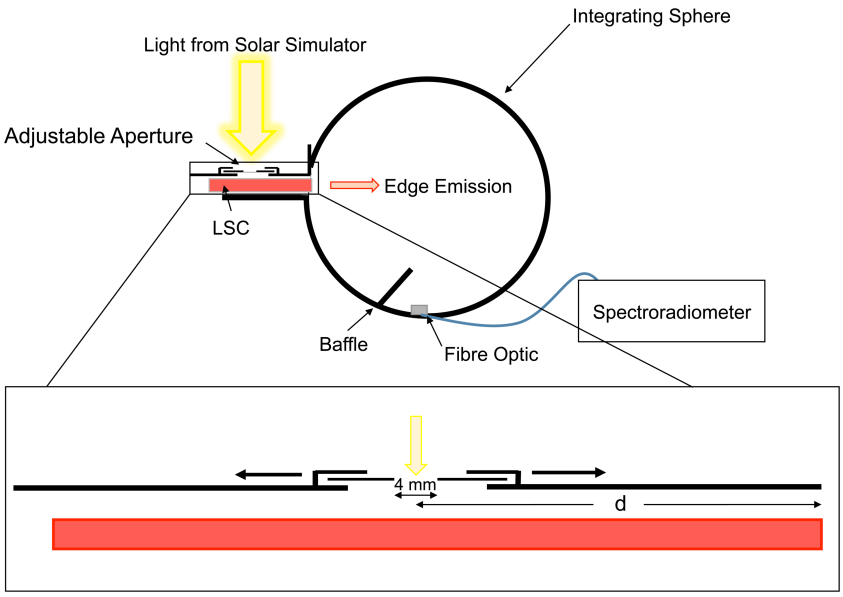

Figure S7. Experimental set-up for determining transport losses in LSCs. A 4 mm diameter irradiation aperture, which can be moved in 1 cm intervals, and a black absorbing mask which completely covers the remainder of the LSC, ensures irradiation at a specific local site. The distance from the LSC edge in integrating sphere to center of aperture is represented here by d.

The experimental set-up used to characterise the optical power output of the LSCs is shown in Figures S6 and S7. Illumination is provided by a Class ABB solar simulator (Abet Technologies, Model 10500), equipped with an AM 1.5 filter and a condenser lens to modify the spectral output of the Xenon lamp to match the solar spectrum at a solar zenith angle of 48.2°. The illumination spot on the LSCs was defined by a black mask with a circular aperture of diameter 3.5 cm. The edge emission of the LSC is directed towards the input port (4 cm diameter) of an integrating sphere, where it is collected and directed to a fiber-optically coupled spectroradiometer (International Light Technologies ILT950). A standard LSC size of 4 × 4 × 0.3 cm was chosen so that the entire edge output can be collected. The emission spectra of the LSCs were recorded over a range of 250-1050 nm using Spectralight software with an ILT1007131U1INS125 manufacturer's calibration file to give the spectral distribution in units of power (μW). The linear attenuation length used to quantify the transport efficiency was measured using the experimental set-up shown in Figure S7. A black mask containing a circular irradiation aperture was used to isolate the irradiation spot (source is the solar simulator). The irradiation spot was moved at fixed distances across the sample surface to enable variation of the detection distance.

(b) Measured optical efficiency of LSCs

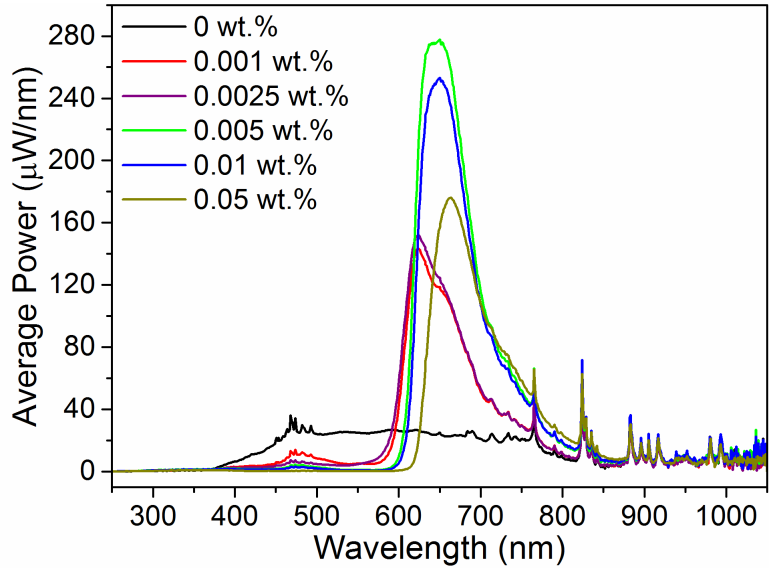

Figure S8. Optical power output of the LSCs with a white scattering background, averaged over all four edges. The noise above 750 nm corresponds to that of the source spectrum.

Table S1. Average power output from the edges of LSCs with different backgrounds and the corresponding total optical efficiencies in wavelength limit: 250 – 1050 nm.

	Absorbing Background		Scattering Background		Scattering Back + Al tape	
Sample Code	Avg. Single Edge Output [mW]	η_{opt} [%]	Avg. Single Edge Output [mW]	η_{opt} [%]	Avg. Single Edge Output [mW]	η_{opt} [%]
0 wt.%	2.9	1.3	11.1	4.9	-	-
0.001 wt.%	7.6	3.4	17.0	7.5	23.7	10.5
0.0025 wt.%	8.6	3.8	17.4	7.7	-	-
0.005 wt.%	17.3	7.7	28.2	12.5	32.2	14.3
0.01 wt.%	16.0	7.1	25.4	11.3	26.2	11.6
0.05 wt.%	13.0	5.8	19.0	8.4	19.8	8.8

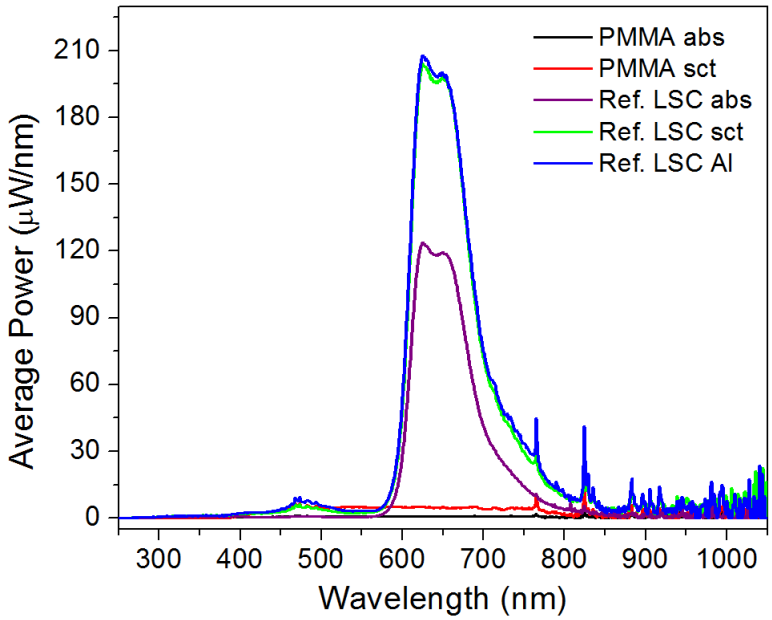

Figure S9. Optical power output of the blank PMMA waveguides and reference thin film LR305/PMMA LSCs. Abs, sct and Al refer to absorbing background, scattering background and scattering background with Al tape, respectively.

Table S2. Average power output from the edges of blank PMMA waveguides and reference thin film LR305-PMMA LSCs and the corresponding total optical efficiencies (η_{opt}).

	Absorbing Background		Scattering Background		Scattering Back + Al tape	
Sample Code	Avg. Single Edge Output [mW]	η_{opt} [%]	Avg. Single Edge Output [mW]	η_{opt} [%]	Avg. Single Edge Output [mW]	η_{opt} [%]
PMMA[a)]	0.5	0.2	2.1	0.9	-	-
Ref. LSC[a)]	11.8	5.2	21.7	9.6	22.3	9.9

[a)] wavelength range: 250 – 1050 nm

S-IV. Spectral estimation of optical loss modes in LSCs

(a) Self-absorption efficiency

The amount of self-absorption in LSCs can be estimated from their edge emission spectra using the method suggested by Dienel *et al*.[1] Assuming that self-absorption causes a red shift in the emission maximum as well as a change in the spectral shape, this method arrives at approximate values for self-absorption efficiency by comparing the observed edge emission spectra with a 'true solution' spectrum that is completely devoid of self-absorption. A solution of the luminophore having an absorbance, A < 0.1 can be can be used as 'true-solution'. By comparing the observed edge spectra with the true solution spectra in the long wavelength region (> 700 nm) where there are no self-absorption effects, a scaling factor is obtained. This scaling factor is used to scale down the observed spectra. The normalized true solution spectrum and the scaled edge emission spectra are shown in Figure S10. Integrating the curves and dividing them as shown in equation (S1) gives the self-absorption efficiency, which represents the light that survives the self-absorption process.

$$\eta_{SA} = \frac{\int_0^\infty S'_{edge}(\lambda)d\lambda}{\int_0^\infty S_{true}(\lambda)d\lambda} \qquad \text{(S1)}$$

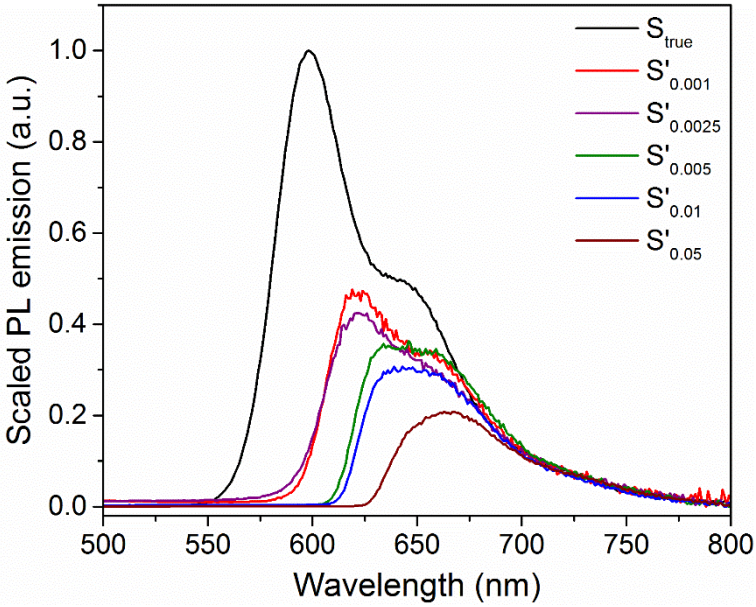

Figure S10. Normalized edge emission spectra of LSCs scaled to match the true emission (dilute solution (S_{true})) spectrum in the 700–800 nm region. $S'_{0.001}$, $S'_{0.005}$ etc. correspond to the edge emission spectra of LSCs with dye concentration of 0.001, 0.005 wt.% *etc.*

(b) Light-Harvesting Efficiency

If the absorbance spectrum A(λ) is known (Figure S11), the light-harvesting efficiency can easily be estimated using the relation

$$\eta_{LHE} = \frac{\int_{w1}^{w2} SS(\lambda)F(\lambda)d\lambda}{\int_{w1}^{w2} SS(\lambda)d\lambda} \qquad \text{(S2)}$$

where $F(\lambda) = [1 - 10^{-A(\lambda)}]$, and SS (λ) represents the solar spectrum. The spectrum of the solar simulator is used as SS (λ) and is shown in grey color in Figure S12.To estimate the light harvesting efficiency using equation (S2), the spectra (SS x F (λ)) shown in Figure S9 are integrated to obtain their mathematical area. Division of these values by the integrated area of the solar simulator spectra (SS), gives the LHE. The wavelength range chosen as the integration limits (w1 to w2) for the above calculation is 300 – 800 nm or 250 – 1000 nm.

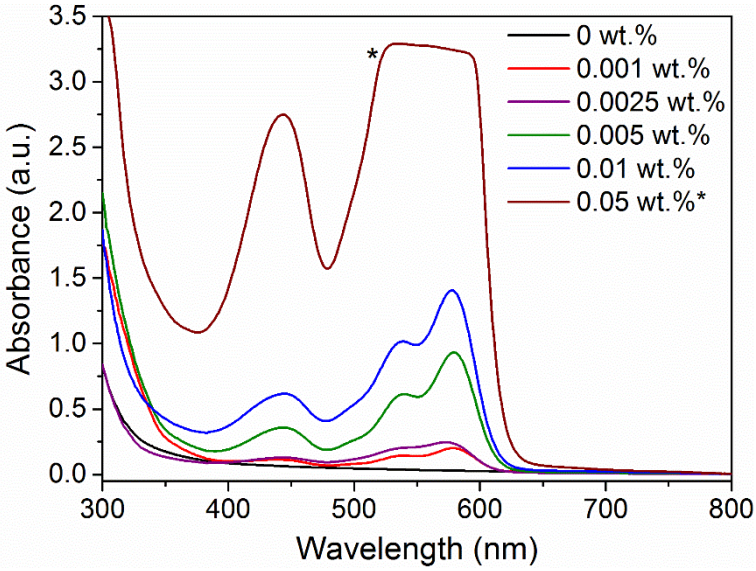

Figure S11. UV/Vis absorbance spectra of LR305-d-U(600) LSCs (size: 4 cm × 4 cm × 3 mm). The absorption spectra of 0.05 wt.% sample is saturated between 500 – 600 nm since the absorbance is very high and beyond the linear response of the detector.

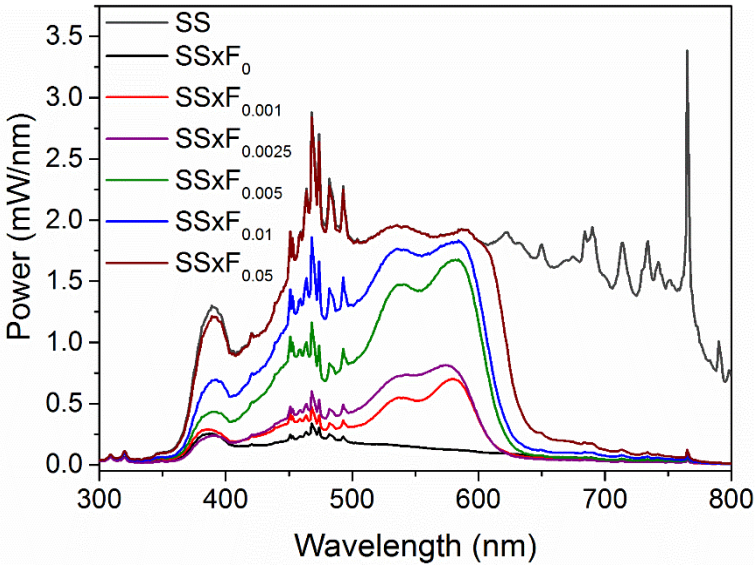

Figure S12. The graphs represent the product of the solar simulator spectrum (SS) and the absorption spectrum $F(\lambda)$ of LR305-d-U(600) LSCs at different luminophore concentrations. $F(\lambda)$ was calculated from the corresponding absorption spectrum $A(\lambda)$ for each LSC.

(c) Luminescent quantum efficiency

Determination of the photoluminescence quantum yield of solid samples becomes difficult due to factors such as non-uniform illumination, waveguiding etc. Use of integrating spheres help in reducing many such issues, however, they introduce an effect of their own. The light emitted from the sample can be re-absorbed due to multiple reflections from highly reflective surface of the sphere. For luminophores exhibiting a low Stokes shift, self-absorption further complicates this process. As a result, the output spectra can undergo reduction in intensity, red-shift of emission maximum and/or change of spectral shape. The corrections suggested by Ahn *et al*.,[2] are similar to those used for determination of self-absorption in LSCs. The difference is that the samples are small in size. Self-absorption is calculated as

$$1-a=\frac{\int_0^\infty S'_{obs}(\lambda)d\lambda}{\int_0^\infty S_{true}(\lambda)d\lambda} \tag{S3}$$

where S_{true} is the emission spectra of a dilute solution of the luminophore and S'_{edge} is the observed emission from the sample scaled to match the true emission spectrum in the long wavelength region, as described in the previous section. The correction factor, a, is used to correct the quantum yield as follows

$$QY=\frac{QY_{obs}}{1-a+aQY_{obs}} \tag{S4}$$

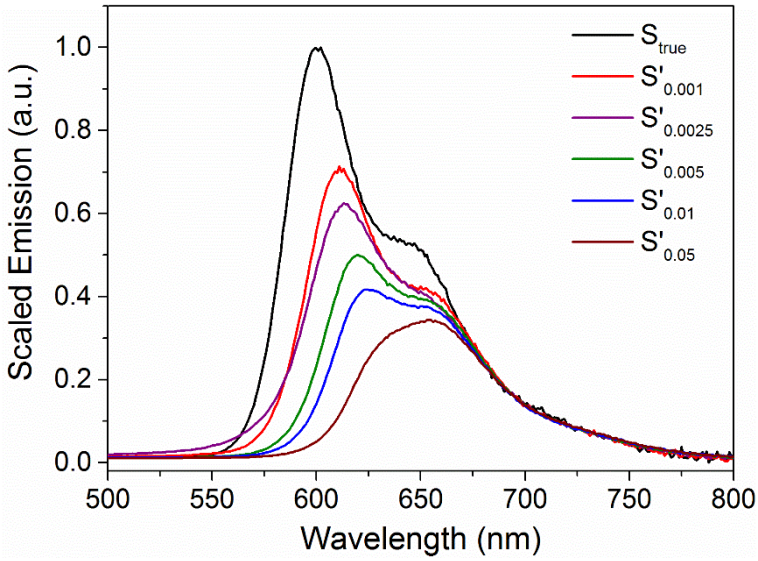

Figure S13. Normalized emission spectra of dilute solution (S_{true}) and the scaled edge emission spectra (S') of LR305-d-U(600) LSC at different luminophore concentrations , scaled to match that of the true emission spectrum in the 700 – 800 nm region.

Table S3. Experimentally determined and corrected quantum yields (PLQY) of LSCs

Sample	Trial 1 [%]	Trial 2 [%]	Trial 3 [%]	Average PLQY [%]	Corrected PLQY [%]
0.001 wt.%	74	73	70	72	77
0.0025 wt.%	74	73	75	74	79
0.005 wt.%	80	81	82	81	88
0.01 wt.%	74	74	77	75	85
0.05 wt.%	58	59	60	59	77

S-V. Mathematics of Efficiency Enhancement Factor

The efficiency enhancement factor defined as

$$E = \frac{\eta_{PV}(\lambda_{em})}{\eta_{PV}(AM1.5G)} \quad \text{(S6)}$$

where $\eta_{PV}(\lambda_{em})$ and $\eta_{PV}(AM1.5G)$ refer to the power conversion efficiencies of the attached solar cell at the emission wavelength of the LSC and under the full solar spectrum, respectively.

The term, E, is related to many equivalent terms used in literature. For example,

1. It is related to the term $\frac{\eta_{solar}}{\eta_{PV}}$ used in many reports[2,5] as $1/E$.

2. It is related to optical collection probability, P[6] as follows:

$$E = \frac{\eta_{PV}(\lambda_{em})}{\eta_{PV}(AM1.5G)} = \frac{\eta_{PCE}(AM1.5G)}{\eta_{PV}(AM1.5G)\cdot\eta_{opt}} = \frac{P}{\eta_{opt}} \quad \text{(S7)}$$

References:

1. T. Dienel, C. Bauer, I. Dolamic, D. Brühwiler, *Sol. Energy* **2010**, *84*, 1366.

2. T. S. Ahn, R. O. Al-Kaysi, A. M. Müller, K. M. Wentz, C. J. Bardeen, *Rev. Sci. Instrum.* **2007**, *78*, 086105.

3. S. F. H. Correia, P. P. Lima, P. S. André, M. R. S. Ferreira, L. A. D. Carlos, *Sol. Energy Mater. Sol. Cells* **2015**, *138*, 51.

4. L. Desmet, A. J. M. Ras, D. K. G. de Boer, M. G. Debije, *Opt. Lett.* **2012**, *37*, 3087.

5. V. T. Freitas, L. Fu, A. M. Cojocariu, X. Cattoën, J. R. Bartlett, R. Le Parc, J.-L. Bantignies, M. Wong Chi Man, P. S. André, R. A. S. Ferreira, L. D. Carlos, *ACS Appl. Mater. Interfaces* **2015**, *7*, 8770.

6. P. T. M. Albers, C. W. M. Bastiaansen, M. G. Debije, *Sol. Energy* **2013**, *95*, 216.